INTERNATIONAL JOURNAL FOR NUMERICAL METHODS IN FLUIDS
Int. J. Numer. Meth. Fluids 2012; **00**:1–33
Published online in Wiley InterScience (www.interscience.wiley.com). DOI: 10.1002/fld

A "well-balanced" finite volume scheme for blood flow simulation

O. Delestre*and P.-Y. Lagrée

CNRS & UPMC Université Paris 06, UMR 7190, 4 place Jussieu, Institut Jean Le Rond d'Alembert, Boîte 162, F-75005 Paris, France

SUMMARY

We are interested in simulating blood flow in arteries with a one dimensional model. Thanks to recent developments in the analysis of hyperbolic system of conservation laws (in the Saint-Venant/ shallow water equations context) we will perform a simple finite volume scheme. We focus on conservation properties of this scheme which were not previously considered. To emphasize the necessity of this scheme, we present how a too simple numerical scheme may induce spurious flows when the basic static shape of the radius changes. On contrary, the proposed scheme is "well-balanced": it preserves equilibria of $Q = 0$. Then examples of analytical or linearized solutions with and without viscous damping are presented to validate the calculations. The influence of abrupt change of basic radius is emphasized in the case of an aneurism.

Received . . .

KEY WORDS: blood flow simulation; well-balanced scheme; finite volume scheme; hydrostatic reconstruction; man at eternal rest; semi-analytical solutions; shallow water

1. INTRODUCTION

As quoted by Xiu and Sherwin [1] the one dimensional system of equations for blood flow in arteries was written long time ago by Leonhard Euler in 1775. Of course, he noticed (see Parker [2]) that it was far too difficult to solve. Since then, the pulsatile wave flow has been understood and is explained in classical books such as Lighthill [3] and Pedley [4]. More recently a huge lot of work has been done and a lot of methods of resolution have been proposed to handle this set of equations, among them [5], [6], [7], [8], [9] [10] [11], [1], [12], [13], [14], [15], [16], [17], [18], [19], [19, 20]... and we forgot a lot of actors. Even if recent progress of fluid structure interaction in 3D have been performed (Gerbeau *et. al.* [21], Van de Vosse *et. al.* [22], among others), those advances have

*Correspondence to: CNRS & UPMC Université Paris 06, UMR 7190, 4 place Jussieu, Institut Jean Le Rond d'Alembert, Boîte 162, F-75005 Paris, France. E-mail: Delestre@unice.fr
Presently at: Laboratoire de Mathématiques J.A. Dieudonné (UMR CNRS 7351) – Polytech Nice-Sophia, Université de Nice – Sophia Antipolis, Parc Valrose, 06108 Nice cedex 02, France

Contract/grant sponsor: This study is part of the ANR ENDOCOM granted by the French National Agency for Research
†Please ensure that you use the most up to date class file, available from the FLD Home Page at
http://www3.interscience.wiley.com/journal/2861/home

not made the 1-D modelisation obsolete. On the contrary, it is needed for validation, for physical comprehension, for boundary conditions, fast or real time computations and it is always relevant for full complex networks of arteries ([6], [7], [23], [8, 24]) or veins ([25]) or in micro circulation in the brain [26].

In most of the previous references it is solved thanks to the method of characteristics, to finite differences or finite volumes (that we will discuss and improve in this paper), or finite elements methods (Galerkin discontinuous). Each method has its own advantages.

In the meanwhile, the set of shallow water equations (though younger, as the equations have been written by Adhémar Barré de Saint-Venant in 1871 [27]) have received a large audience as well. They are used for modelling the flow in rivers [28], [29] (and networks of rivers), in lakes, rain overland flow [30, 31], [32], in dams [33, 34] or the long waves in shallow water seas (tides in the Channel for example [35], or for Tsunami modelling [36], [37]). It has been observed that Saint-Venant equations with source terms (which are the shape of the topography, and the viscous terms) present numerical difficulties for steady states. The splitting introduced by the discretisation creates an extra unphysical flow driven by the change of the topography. A configuration with no flow, for example a lake, will not stay at rest: thus, the so called equilibrium of the "lake at rest" is not preserved. So new schemes, called "well-balanced" have been constructed to preserve this equilibrium. Bermudez and Vazquez [38, 39] have modified the Roe solver to preserve steady states. Other ways to adapt exact or approximate Riemann solver to non-homogeneous case have been proposed by LeVeque [40] and Jin [41]. Following the idea of the pioneer work of Greenberg and LeRoux [42], [43] and [44] have proposed schemes based on the solution of the Riemann problem associated with a larger system (a third equation on the bottom topography variable is added). A central scheme approach has been developped in [45]. In Perthame and Simeoni [46], the source terms are included in the kinetic formulation. In [47] and [48], a well-balanced hydrostatic reconstruction has been derived. It can be applied to any conservative finite volume scheme approximating the homogeneous Saint-Venant system. In [49], [50], [48] and [51, 52] the friction source term is treated under a well-balanced way. More recently, in [53], the system of shallow water with topography is rewritten under a homogeneous form. This enables them to get Lax-Wendroff and MacCormack well-balanced schemes. With well-balanced methods, spurious current does not appear.

Thus we will follow those authors and construct by analogy a similar method but for flows in elastic tubes rather than for free surface flows. Even if for artery flows the wave behaviour of the solution is very important (forced regime with lot of reflexions), we have in mind complex networks. In this case we will have to deal from the arteries to the veins with eventually microcirculation in the brain. In the smaller and softer vessels, the 1D approximation is still valid, the pulsatile behaviour is less important, and there are lot of changes of sections (across stenosis, aneurisms, valves). Those changes of sections have to be treated numerically with great care, which has not been the case up to now in the litterature.

So here, we will follow the authors of the Saint-Venant community and construct by analogy a similar method but for artery flow. At first we derive the equations written in conservative form, looking in the literature, we found that it has been only written by [13] in a PhD thesis and by [16], [18] but not exploited in the "well-balanced" point of view. Mostly ([1], [20]), equations are in fact written in a non-conservative form. With non-conservative schemes, we have consistency

DOI: 10.1002/fld

defaults and shocks are not uniquely defined, see among others [54], [55] and [56]. Furthermore, the discharge Q is not conserved. Not a lot of attention has been attached to this problem up to now. But this non conservation is a real problem if we consider networks with tubes with non uniform section and ultimately quasi steady flow in small terminal vessels.

Hence after the introduction of the set of equations in section 2 and deriving with this new point of view the conservative equations, we construct by analogy the numerical scheme both at first and second order in section 3. Then section 4 is devoted to several test cases to validate the different parts of the equations. The most important case is the "man at eternal rest" by analogy to the "lake at rest" which would not be preserved by non-conservative schemes. The aim of this paper is to use this property to construct efficient methods of resolution.

2. THE 1D MODEL

2.1. Derivation of the equations

We first derive the model equations, they are of course now classical, as already mentioned. Starting from unsteady incompressible axi-symmetrical Navier-Stokes equations, and doing a long wave approximation one obtains a first set of Reduced Navier-Stokes equations ([10], [57]). One has the longitudinal convective term, the longitudinal pressure gradient, and only the transverse viscous term, the longitudinal being negligible. The pressure is constant across the cross section and depends only of x the longitudinal variable. The incompressibility is preserved.

Then, integrating over the section, one obtains two integrated equations (kind of Von Kármán equation). The first one is obtained from incompressibility and application of boundary condition and relates the variation of section to the variations of flow. The second one is obtained from the momentum. The final equations are not closed and one has to add some hypothesis on the shape of the velocity profile to obtain a closed system (some discussions of this are in [10]). We then obtain the following system with dimensions which is the 1-D model of flow:

$$\begin{cases} \partial_t A + \partial_x Q = 0 \\ \partial_t Q + \partial_x \dfrac{Q^2}{A} + \dfrac{A}{\rho}\partial_x p = -C_f \dfrac{Q}{A} \end{cases}, \tag{1}$$

where $A(x,t)$ is the cross-section area ($A = \pi R^2$, where R is the radius of the vessel), $Q(x,t) = A(x,t)u(x,t)$ is the flow rate or the discharge, $u(x,t)$ the mean flow velocity, and ρ the blood density (see figure 1). The first equation is without any approximation. An extra factor of value $4/3$ may appear in front of Q^2/A if the chosen profile is a Poiseuille profile (with either large viscosity ν or low frequency $\omega/(2\pi)$ so that $\alpha = R_0\sqrt{\omega/\nu}$ the Womersley number is small). This comes from the fact that this term is in fact an approximation of $\int_0^R 2\pi u(t,x,r)^2 r dr$ (this $u(t,x,r)$ being the actual longitudinal velocity, not to be confused with $u(x,t) = \int_0^R 2\pi u(t,x,r) r dr$). The chosen unit value corresponds to a flat profile. The viscous term has been modelised by a friction proportional to Q/A (see [58] [10]): $C_f = 8\pi\nu$ where ν is the blood viscosity. Again, a friction term written $-8\pi\nu Q/A$ is an approximation of the effective term which is $\nu R\partial u/\partial r|_R$ (with here again $u(t,x,r)$ the real longitudinal velocity). This specific choice corresponds to a Poiseuille flow

DOI: 10.1002/fld

(small α), and is therefore non consistent with the coefficient in the convective term. This is not a real problem, those coefficients are adjusted in the literature. Note that in Saint-Venant community, the skin friction modelling involves a square of Q, reminiscent to the turbulent nature of river flow. This is seldom used in blood-flow. To conclude on the mechanical modelling we will take the form of Eq. 1 for granted and we will no more discuss it.

Finally, one has to model the arterial wall, the pressure has to be linked with the displacement of the vessel. A simple elastic linear term in the variation of radius is taken:

$$p - p_0 = k(R - R_0) \text{ or as well } p = p_0 + k\frac{\sqrt{A} - \sqrt{A_0}}{\sqrt{\pi}}, \tag{2}$$

$A_0(x)$ is the cross section at rest ($A_0 = \pi R_0^2$, where R_0 is the radius of the vessel which may be variable in the case of aneurism, stenosis or taper), and the stiffness k is taken as a constant. The external pressure p_0 is supposed constant as well. Again, this relation which is here a simple elastic string model may be enhanced. Non linear terms, non local (tension) terms and/or dissipative unsteady terms may be introduced (viscoelasticity). We take here the most simple law, but we are aware of the possibilities of complexity.

Note that the derivation of those equations may be done with only 1D fluid mechanics arguments ([26] or [59]). One has to be very careful then to write precisely the action of the pressure on the lateral walls (for example Kundu [60] page 793 does a mistake in his text book). But, the real point of view to derive the equations is the one explained at the beginning of this section and involves the Reduced Navier-Stokes equations ([10]).

We will now change a bit this form to write a real conservative form. Note that authors ([11], [20]) write system (1) as

$$\partial_t U + \partial_x F(U) = S(U),$$

they use the variables $U = (A, u)$, so that they identify a kind of flux $F(U) = (Au, u^2/2 + p/\rho)$ and a source term $S(U) = -C_f u/A$. But u is not a conservative quantity, Q is, as we will see next.

Of course, those Saint-Venant and blood flow equations are very similar to the 1D Euler compressible equations that one can write in nozzles, or in acoustics (Lighthill [3]), in this case the density ρ is variable and linked to the pressure by the isentropic law $p \propto \rho^\gamma$. This relation is the counter part of the relation of pressure which are in Saint-Venant and respectively in the artery: hydrostatic balance $p = \rho g \eta$ (density, gravitational acceleration, level of the free surface) and respectively the elasticity response of the artery $p = k(R - R_0)$ (stiffness of the wall, current radius of the vessel, reference radius at rest).

2.2. *Conservative system*

So, to write the conservative system, the second equation of (1) is rewritten and developed. Thus we get the following system of conservation laws:

$$\begin{cases} \partial_t A + \partial_x Q = 0 \\ \partial_t Q + \partial_x \left[\dfrac{Q^2}{A} + \dfrac{k}{3\rho\sqrt{\pi}} A^{3/2} \right] = \dfrac{kA}{2\rho\sqrt{\pi}\sqrt{A_0}} \partial_x A_0 - C_f \dfrac{Q}{A} \end{cases}, \tag{3}$$

DOI: 10.1002/fld

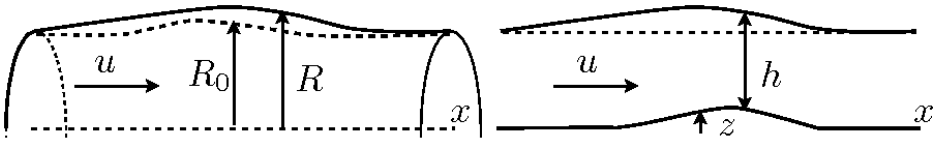

Figure 1. 1D models: left the blood flow model (u is the mean velocity, R the radius, $A = \pi R^2$ the instantaneous area, R_0 the radius at rest, $A_0 = \pi R_0^2$ the area with no flow), right the shallow water model (u is the mean velocity, h the water column height, z the topography).

we can write (3) under a more compact form:

$$\partial_t U + \partial_x F(U) = S(U), \tag{4}$$

with a new definition of U, $F(U)$ and $S(U)$. We identify U the vector of the conservative variables, $F(U)$ the flux

$$U = \begin{pmatrix} A \\ Q \end{pmatrix}, \; F(U) = \begin{pmatrix} Q \\ \dfrac{Q^2}{A} + \dfrac{k}{3\rho\sqrt{\pi}} A^{3/2} \end{pmatrix} \tag{5}$$

and the source term takes into account the initial shape of the vessel A_0 and the friction term:

$$S(U) \quad = \begin{pmatrix} 0 \\ \dfrac{kA}{\rho\sqrt{\pi}} \partial_x \sqrt{A_0} - C_f \dfrac{Q}{A} \end{pmatrix}. \tag{6}$$

This system is strictly hyperbolic when $A > 0$ (which should be the case in arteries). Indeed, this means that we have

$$\partial_x F(U) = \begin{pmatrix} 0 & 1 \\ \dfrac{k\sqrt{A}}{2\rho\sqrt{\pi}} - \dfrac{Q^2}{A^2} & \dfrac{2Q}{A} \end{pmatrix} . \partial_x \begin{pmatrix} A \\ Q \end{pmatrix} = J(U) . \partial_x U,$$

where the Jacobian matrix $J(U)$ has two real eigenvalues (which is the definition of hyperbolicity)

$$\lambda_1 = \frac{Q}{A} - \sqrt{\frac{k\sqrt{A}}{2\rho\sqrt{\pi}}} = u - c \quad \text{and} \quad \lambda_2 = \frac{Q}{A} + \sqrt{\frac{k\sqrt{A}}{2\rho\sqrt{\pi}}} = u + c. \tag{7}$$

We recognise c as the well-known Moens Korteweg wave propagation speed ([4]):

$$c = \sqrt{\frac{k\sqrt{A}}{2\rho\sqrt{\pi}}}.$$

The system (3) without friction *i.e.* with $C_f = 0$ admits special solutions which are steady state solutions, that means that we have

$$\partial_t A = \partial_t u = \partial_t Q = 0. \tag{8}$$

DOI: 10.1002/fld

Thus the mass conservation equation gives the discharge conservation: $\partial_x Q(x,t) = 0$. The momentum conservation equation, under the steady state and frictionless hypothesis reduces to

$$\partial_x \left[\frac{{Q_0}^2}{2A^2} + b\sqrt{A} - b\sqrt{A_0} \right] = 0, \tag{9}$$

with $b = k/(\rho\sqrt{\pi})$. So that system (3) integrates to the two constants:

$$\left\{ \begin{array}{l} Q(x,t) = Q_0 \\ \dfrac{{Q_0}^2}{2A^2} + b\sqrt{A} - b\sqrt{A_0} = Cst \end{array} \right. . \tag{10}$$

The first is a constant flux, the second is the Bernoulli constant.

We have of course made analogy between (3) and the one-dimensional Saint-Venant (or shallow water) system:

$$\left\{ \begin{array}{l} \partial_t h + \partial_x q = 0 \\ \partial_t q + \partial_x \left(\dfrac{q^2}{h} + \dfrac{gh^2}{2} \right) = -gh\partial_x z - c|q| \dfrac{q}{h^\beta} \end{array} \right. , \tag{11}$$

where $h(x,t)$ is the water height, $u(x,t)$ the mean flow velocity, $q(x,t) = h(x,t)u(x,t)$ the flow rate and $z(x,t)$ the topography of the bottom and c is the friction coefficient. With $\beta = 2$ we recover Chezy's or Darcy-Weisbach's law (depending on the way c is written) and with $\beta = 7/3$, we get the Manning-Strickler's friction law.

This system admits steady state frictionless solutions too:

$$\partial_t h = \partial_t u = \partial_t q = 0. \tag{12}$$

Thus we get the conservation of discharge and the Bernoulli's relation

$$\left\{ \begin{array}{l} q = q_0 \\ \dfrac{{q_0}^2}{2gh^2} + z + h = Cst \end{array} \right. , \tag{13}$$

which is the exact analogous of (10). In the literature we can find numerical schemes preserving steady states under the form (13), but they are complex to handle (see [61], [62], [63] and [64]). Most of the time, more simple steady states are considered

$$\left\{ \begin{array}{l} q = u = 0 \\ \partial_x \left(g\dfrac{h^2}{2} \right) + gh\partial_x z = 0 \end{array} \right. , \tag{14}$$

which correspond from a mechanical point of view to the modelling of a "lake at rest". We have a balance called hydrostatic balance between the hydrostatic pressure and the gravitational acceleration down an inclined bottom z. The second term of (14) reduces to

$$H = h + z = Cst, \tag{15}$$

DOI: 10.1002/fld

where H is the water level. Since the work of [42], schemes preserving at least (14) are called well-balanced schemes. This allows to have an efficient treatment of the source term. Thus, in practice, schemes preserving (14) give good results even in unsteady cases. The analogous of the "lake at rest" for the system (3) without friction, can be called the "man at eternal rest" or "dead man equilibrium", it writes

$$\begin{cases} Q = u = 0 \\ \partial_x \left(\dfrac{k}{3\rho\sqrt{\pi}} A^{3/2} \right) - \dfrac{kA}{\rho\sqrt{\pi}} \partial_x \sqrt{A_0} = 0 \end{cases} . \tag{16}$$

In this case we have $\sqrt{A} = \sqrt{A_0}$. We will now use this property to construct the schemes.

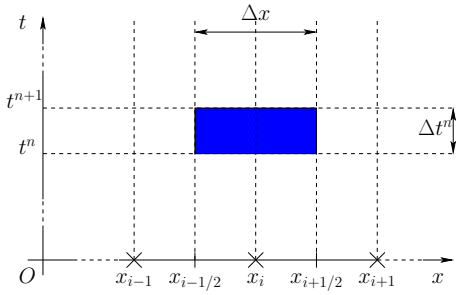

Figure 2. The time and space stencils.

3. THE NUMERICAL METHOD

In this section, we describe the scheme for system (1) at first and second order, with the space and time discretisation illustrated in Figure 2.

3.1. Convective step

For the homogeneous system *i.e.* system (4) without source term: $S(U) = 0$, a first-order conservative finite volume scheme writes simply (see figure 2):

$$\frac{U_i^{n+1} - U_i^n}{\Delta t} + \frac{F_{i+1/2}^n - F_{i-1/2}^n}{\Delta x} = 0, \tag{17}$$

where U_i^n is an approximation of U

$$U_i^n \simeq \frac{1}{\Delta x} \int_{x_{i-1/2}}^{x_{i+1/2}} U(x, t_n) dx$$

n refers to time t_n with $t_{n+1} - t_n = \Delta t$ and i to the cell $C_i = (x_{i-1/2}, x_{i+1/2}) = (x_{i-1/2}, x_{i-1/2} + \Delta x)$. The two points numerical flux $F_{i+1/2}$ is an approximation of the flux function (5) at the cell interface $i + 1/2$

$$F_{i+1/2} = \mathcal{F}(U_i, U_{i+1}). \tag{18}$$

This flux function will be detailed in section 3.3.

DOI: 10.1002/fld

3.2. Source term treatment

3.2.1. "Topography" treatment The source term $\frac{kA}{\rho\sqrt{\pi}}\partial_x\sqrt{A_0}$ is the analogous of the topography source term $(-gh\partial_x z)$ in the shallow water system (11). Looking at (3), it might be treated explicitly which writes

$$U_i^{n+1} = U_i^n - \frac{\Delta t}{\Delta x}\left(F_{i+1/2}^n - F_{i-1/2}^n\right) + \Delta t S(U_i^n) \tag{19}$$

where the source is written simply by evaluating the derivative of A_0:

$$S(U_i^n) = \begin{pmatrix} 0 \\ \dfrac{kA_i^n}{2\rho\sqrt{\pi}\sqrt{A_{0i}}}\dfrac{A_{0i+1/2} - A_{0i-1/2}}{\Delta x} \end{pmatrix},$$

with the definition

$$A_{0i+1/2} = \frac{A_{0i+1} + A_{0i}}{2}.$$

We will illustrate the fault of this naive method in sections 4.4 and 4.5. We will prefer a well-balanced method inspired from the hydrostatic reconstruction (see [47] and [48]). As for the hydrostatic reconstruction we do not consider the friction term and we are looking for a scheme which preserves steady states at rest (16), the second equation in (16) means that we have

$$\sqrt{A} - \sqrt{A_0} = Cst, \tag{20}$$

as for the hydrostatic reconstruction we will use locally this relation to perform a reconstruction of the variable A. On each part of the interface, we have the following reconstructed variables

$$\begin{cases} \sqrt{A_{i+1/2L}} = \max(\sqrt{A_i} + \min(\Delta\sqrt{A_0}_{i+1/2}, 0), 0) \\ U_{i+1/2L} = (A_{i+1/2L}, A_{i+1/2L}u_i)^t \\ \sqrt{A_{i+1/2R}} = \max(\sqrt{A_{i+1}} - \max(\Delta\sqrt{A_0}_{i+1/2}, 0), 0) \\ U_{i+1/2R} = (A_{i+1/2R}, A_{i+1/2R}u_{i+1})^t \end{cases}, \tag{21}$$

where $\Delta\sqrt{A_0}_{i+1/2} = \sqrt{A_{0i+1}} - \sqrt{A_{0i}}$.

For consistency the scheme (17) has to be slightly modified under the form

$$U_i^{n+1} = U_i^n - \frac{\Delta t}{\Delta x}(F_{i+1/2L}^n - F_{i-1/2R}^n), \tag{22}$$

where

$$\begin{array}{l} F_{i+1/2L}^n = F_{i+1/2}^n + S_{i+1/2L} \\ F_{i-1/2R}^n = F_{i-1/2}^n + S_{i-1/2R} \end{array}, \tag{23}$$

with

$$\begin{array}{l} S_{i+1/2L} = \begin{pmatrix} 0 \\ \mathcal{P}(A_i^n) - \mathcal{P}(A_{i+1/2L}^n) \end{pmatrix} \\ S_{i-1/2R} = \begin{pmatrix} 0 \\ \mathcal{P}(A_i^n) - \mathcal{P}(A_{i-1/2R}^n) \end{pmatrix} \end{array} \tag{24}$$

and

$$\mathcal{P}(A) = \frac{k}{3\rho\sqrt{\pi}}A^{3/2}. \tag{25}$$

DOI: 10.1002/fld

The numerical flux $F^n_{i+1/2}$ is now calculated with the reconstructed variables (21):

$$F^n_{i+1/2} = \mathcal{F}(U^n_{i+1/2L}, U^n_{i+1/2R}).$$

Having treated the term linked to the variation of radius we now turn to the friction term.

3.2.2. Friction treatment Concerning the friction treatment two methods are presented here, namely: a semi-implicit treatment ([65], [66], and [67]) which is classical in shallow water simulations and the apparent topography method (see [48], [68, 69]) which is a well-balanced method.

Semi-implicit treatment We use (22) as a prediction without friction, *i.e.*:

$$U^*_i = U^n_i - \frac{\Delta t}{\Delta x}(F^n_{i+1/2L} - F^n_{i-1/2R}) \tag{26}$$

and a friction correction (via a semi-implicit treatment) is applied on the predicted variables (U^*_i):

$$A^*_i \left(\frac{u^{n+1}_i - u^*_i}{\Delta t} \right) = -C_f u^{n+1}_i, \tag{27}$$

thus we get u^{n+1}_i and we have $A^{n+1}_i = A^*_i$. It preserves zero velocity.

Apparent topography The apparent topography method (see [48]) consists in writing the second equation of the system under the following form

$$\partial_t Q + \partial_x \left[\frac{Q^2}{A} + \frac{k}{3\rho\sqrt{\pi}} A^{3/2} \right] = \frac{kA}{\rho\sqrt{\pi}} \partial_x \sqrt{A_{0app}}, \tag{28}$$

with

$$\partial_x \sqrt{A_{0app}} = \partial_x \left(\sqrt{A_0} + b \right),$$

where

$$\partial_x b = -\frac{\rho\sqrt{\pi} C_f}{k} \frac{Q}{A^2}.$$

The hydrostatic reconstruction (21) is performed with the corrected term $\sqrt{A_{0app}}$.

3.3. Numerical flux

Several numerical fluxes might be used, some of them are defined in the following.

Rusanov flux Following [48], the Rusanov flux writes

$$\mathcal{F}(U_L, U_R) = \frac{F(U_L) + F(U_R)}{2} - c \frac{U_R - U_L}{2},$$

with

$$c = \sup_{U = U_L, U_R} \left(\sup_{j \in \{1,2\}} |\lambda_j(U)| \right),$$

DOI: 10.1002/fld

where $\lambda_1(U)$ and $\lambda_2(U)$ are the eigenvalues of the system.

HLL flux Following [48], the HLL flux (Harten, Lax and van Leer [70]) writes

$$\mathcal{F}(U_L,U_R)=\begin{cases} F(U_L) & \text{if } 0\leq c_1 \\ \dfrac{c_2F(U_L)-c_1F(U_R)}{c_2-c_1}+\dfrac{c_1c_2}{c_2-c_1}(U_R-U_L) & \text{if } c_1<0<c_2 \\ F(U_R) & \text{if } c_2\leq 0 \end{cases}, \tag{29}$$

with

$$c_1=\inf_{U=U_L,U_R}\left(\inf_{j\in\{1,2\}}\lambda_j(U)\right) \text{ and } c_2=\sup_{U=U_L,U_R}\left(\sup_{j\in\{1,2\}}\lambda_j(U)\right),$$

where $\lambda_1(U)$ and $\lambda_2(U)$ are the eigenvalues of the system.

VFRoe-ncv flux Adapting the main line of [71] and [72], we get the following VFRoe-ncv flux for system (3)

$$\mathcal{F}(U_L,U_R)=\begin{cases} F(U_L) \text{ if } 0\leq\lambda_1(\widetilde{U}) \\ F(U_*) \text{ if } \lambda_1(\widetilde{U})<0<\lambda_2(\widetilde{U}) \\ F(U_R) \text{ if } \lambda_2(\widetilde{U})\leq 0 \end{cases},$$

with the mean state

$$\widetilde{W}=\begin{pmatrix} 4\tilde{c} \\ \tilde{u} \end{pmatrix}=\begin{pmatrix} 2\left(c_L+c_R\right) \\ \dfrac{u_L+u_R}{2} \end{pmatrix}$$

and

$$U_*=\begin{pmatrix} A_* \\ A_*u_* \end{pmatrix},$$

where A_* et u_* are the Roe mean states, we get them thanks the Riemann invariant

$$\begin{cases} u_R-4c_R=u_*-4c_* \\ u_L+4c_L=u_*+4c_* \end{cases}, \tag{30}$$

thus we have

$$\begin{cases} u_*=\tilde{u}-2(c_R-c_L) \\ c_*=\tilde{c}-\dfrac{1}{8}(u_R-u_L) \end{cases}.$$

When $\lambda_1(U_L)<0<\lambda_1(U_R)$ or $\lambda_2(U_L)<0<\lambda_2(U_R)$, we can get non entropic solutions. We perform an entropy correction thanks to the Rusanov flux.

Kinetic flux Adapting the main line of [73] and [74], we get the following kinetic flux for system (3)

$$\mathcal{F}(U_L,U_R)=F_+(U_L)+F_-(U_R),$$

with

$$F_+(U_L)=\frac{A_L}{2\sqrt{3T_L}}\begin{pmatrix} \dfrac{{M_+}^2-{M_-}^2}{2} \\ \dfrac{{M_+}^3-{M_-}^3}{3} \end{pmatrix}$$

DOI: 10.1002/fld

$$F_-(U_R) = \frac{A_R}{2\sqrt{3T_R}} \begin{pmatrix} \dfrac{{m_+}^2 - {m_-}^2}{2} \\ \dfrac{{m_+}^3 - {m_-}^3}{3} \end{pmatrix}$$

where

$$\begin{cases} M_+ = \max(0, u_L + \sqrt{3T_L}) \\ M_- = \max(0, u_L - \sqrt{3T_L}) \\ m_+ = \min(0, u_R + \sqrt{3T_R}) \\ m_- = \min(0, u_R - \sqrt{3T_R}) \end{cases}$$

with

$$T_L = \frac{k}{3\rho\sqrt{\pi}}\sqrt{A_L} \quad \text{and} \quad T_R = \frac{k}{3\rho\sqrt{\pi}}\sqrt{A_R}.$$

CFL condition We have to impose a CFL (Courant, Friedrichs, Levy) condition on the timestep to prevent blow up of the numerical values and to ensure the positivity of A. This classical stability condition writes

$$\Delta t \leq n_{CFL} \frac{\min\limits_i(\Delta x_i)}{\max\limits_i(|u_i| + c_i)},$$

where $c_i = \sqrt{k\sqrt{A_i}/(2\rho\sqrt{\pi})}$ and $n_{CFL} = 1$ (resp. $n_{CFL} = 0.5$) for the first order scheme (resp. for the second order scheme see 3.5).

We have to notice that the kinetic flux needs a particular CFL condition (see [73, p.24])

$$\Delta t \leq n_{CFL} \frac{\min\limits_i(\Delta x_i)}{\max\limits_i(|u_i| + \sqrt{3T_i})}.$$

The Rusanov is the most diffusive but the most simple to implement, the kinetic one is slightly less diffusive but more cpu time consuming. VFRoe-ncv and HLL are comparable, but the first one is a little more time consuming due to entropy correction. All these fluxes are compared in [75] in Saint-Venant framework.

3.4. Boundary conditions

3.4.1. Characteristic system Of course boundary conditions are very important for artery flow. We will not too much insist on them, and we will not present for example the classical Windkessel model or variations. Nevertheless, adapting [66] to blood flow, we can write the homogeneous form of (4) under the following non conservative form

$$\begin{cases} \partial_t A + u\partial_x A + A\partial_x u = 0 \\ \partial_t u + \dfrac{k}{2\rho\sqrt{\pi}\sqrt{A}}\partial_x A + u\partial_x u = 0 \end{cases}. \tag{31}$$

Thanks to the Moens Korteweg velocity rewritten as $A = c^4\pi(2\rho/k)^2$, we get

$$\begin{cases} \partial_t \left[4c - u\right] + (u - c)\partial_x \left[4c - u\right] = 0 \\ \partial_t \left[4c + u\right] + (u + c)\partial_x \left[4c + u\right] = 0 \end{cases}, \tag{32}$$

DOI: 10.1002/fld

thus we have $\frac{d(4c-u)}{dt}=0$ (respectively $\frac{d(4c+u)}{dt}=0$) or the Riemann invariant $4c-u=Cst$ (resp. $4c+u=Cst$) along the characteristic curve C_- (resp. C_+) defined by the equation $\frac{dx}{dt}=u-c$ (resp. $\frac{dx}{dt}=u+c$).

The boundary conditions will be prescribed thanks to the method of characteristics. We set $U_{bound}=U(0)$ or $U(L)$ and $U_{near}=U(\Delta x)$ or $U(L-\Delta x)$ depending on the considered boundary ($x=0$ or $x=L$).

3.4.2. Subcritical flow We write here boundary condition for subcritical flow: at the boundary the flow is subcritical if we have $|u_{bound}|<c_{bound}$ or equivalently

$$(u_{bound}-c_{bound})\,(u_{bound}+c_{bound})<0. \tag{33}$$

Of course it seems to be always the case in blood flows, where $|Q/(Ac)|$ is less than 10 % in physicological cases. This concept is more relevant to Saint-Venant equation, where supercritical flow are easily obtained. Two cases are possible: we are given either the cross section A (the pressure thanks to (2)) or the discharge Q.

- Given cross section $A_{bound}=Cst$:
  At $x=0$ the Riemann invariant is constant along the ingoing characteristic $u-c$, thus we have
  $$\left\{\begin{array}{l} A_{bound}=Cst \\ u_{bound}=u_{near}-4\left[c_{near}-c_{bound}\right] \end{array}\right. . \tag{34}$$
  At $x=L$ the Riemann invariant is constant along the outgoing characteristic $u+c$, thus we have
  $$\left\{\begin{array}{l} A_{bound}=Cst \\ u_{bound}=u_{near}+4\left[c_{near}-c_{bound}\right] \end{array}\right. . \tag{35}$$
  If (33) is not verified by the couple (A_{bound},u_{bound}), the flow is in fact supercritical.
- Given discharge $Q_{bound}=Cst$:
  Depending on the boundary considered we have either at $x=0$
  $$0=-Q_{bound}+(u_{near}-4c_{near})A_{bound}+4c_{bound}A_{bound}, \tag{36}$$
  or at $x=L$
  $$0=-Q_{bound}+(u_{near}+4c_{near})A_{bound}-4c_{bound}A_{bound}. \tag{37}$$
  We recall that c_{bound} depends on A_{bound}, we solve (36) or (37) to get A_{bound}.

The source terms might be considered negligible in the characteristic method.

3.4.3. Supercritical flow As previously mentioned, this is not really a relevant case for flows in arteries. But, in veins, or in collapsible tubes, it may be relevant (see Pedley [4]). A supercritical inflow corresponds to both $A_{bound}=Cst_1$ and $Q_{bound}=Cst_2$ that have to be imposed. A supercritical outflow is such that we have $A_{bound}=A_{near}$ and $Q_{bound}=Q_{near}$.

Again, source terms are neglected in the characteristic method.

DOI: 10.1002/fld

In order to impose the discharge $Q_{bound} = A_{bound}u_{bound}$, we can use an other method: the use of the first component of the numerical flux is an accurate way to proceed, even if $\mathcal{F}_1(U_L, U_R) = Q_{bound}(t)$ has no unique solution (and the complexity of the problem depends on the numerical flux).

3.5. Second order scheme

In order to get a second order scheme, we use the following algorithm:

Step 1 In order to get second order reconstructed variables $\left(U_{\bullet\pm}, \sqrt{A_0}_{\bullet\pm}\right)$ we perform a linear reconstruction on variables u, A, $\sqrt{A} - \sqrt{A_0}$ then we get the reconstruction on $\sqrt{A_0}$.

We consider the scalar function $s \in \mathbb{R}$, its linear reconstruction is defined by

$$s_{i-1/2+} = s_i - \frac{\Delta x}{2} D s_i \quad \text{and} \quad s_{i+1/2-} = s_i + \frac{\Delta x}{2} D s_i$$

where D is one of the following reconstruction operator D_{muscl}, D_{eno} and D_{enom}. To get the reconstruction operator D, we introduce the minmod slope limiter

$$\text{minmod}(x, y) = \begin{cases} \min(x, y) & \text{if } x, y \geq 0 \\ \max(x, y) & \text{if } x, y \leq 0 \\ 0 & \text{else} \end{cases}.$$

Some other slope limiters might be found in [76, p.111-112] (the Monotonized Central difference limiter and the Superbee limiter).

MUSCL With the operator

$$D_{muscl} s_i = \text{minmod}\left(\frac{s_i - s_{i-1}}{\Delta x}, \frac{s_{i+1} - s_i}{\Delta x}\right),$$

we get the MUSCL linear reconstruction (Monotonic Upwind Scheme for Conservation Law [77]). We can find a less diffusive but more complicated form of the MUSCL reconstruction in [78].

ENO With the operator

$$D_{eno} s_i = \text{minmod}\left(\frac{s_i - s_{i-1}}{\Delta x} + \theta_{eno}\frac{\Delta x}{2} D^2 s_{i-1/2}, \frac{s_{i+1} - s_i}{\Delta x} + \theta_{eno}\frac{\Delta x}{2} D^2 s_{i+1/2}\right),$$

where

$$D^2 s_{i+1/2} = \text{minmod}\left(\frac{s_{i+1} - 2s_i + s_{i-1}}{\Delta x^2}, \frac{s_{i+2} - 2s_{i+1} + s_i}{\Delta x^2}\right)$$

and

$$\theta_{eno} = 1,$$

we perform the ENO linear reconstruction (Essentially Non Oscillatory [79, 80], [81]). This reconstruction is more accurate than the MUSCL reconstruction but less stable. In order to get a more stable reconstruction we can take θ_{eno} in $[0, 1]$ (it is recommended to take $\theta_{eno} = 0.25$ [82, p.236]).

DOI: 10.1002/fld

modified ENO With the operator

$$D_{enom}s_i = \text{minmod}\left(D_{eno}s_i, 2\theta_{enom}D_{muscl}s_i\right), \text{ with } \theta_{enom} \in [0,1],$$

we get the modified ENO linear reconstruction [48, p.55-56] and [82, p.235-237].

The previous linear reconstructions applied to A writes

$$A_{i-1/2+} = A_i - \frac{\Delta x}{2}DA_i,\ A_{i+1/2-} = A_i + \frac{\Delta x}{2}DA_i,$$

thus we have the following conservation relation

$$\frac{A_{i-1/2+} + A_{i+1/2-}}{2} = A_i.$$

In order to get the same kind of relation on the discharges, the following modified reconstruction is performed on the velocity variables u

$$u_{i-1/2+} = u_i - \frac{A_{i+1/2-}}{A_i}\frac{\Delta x}{2}Du_i,\ u_{i+1/2-} = u_i + \frac{A_{i-1/2+}}{A_i}\frac{\Delta x}{2}Du_i,$$

this allows to get the conservation relation

$$\frac{A_{i-1/2+}u_{i-1/2+} + A_{i+1/2-}u_{i+1/2-}}{2} = A_iu_i.$$

We perform on $\Psi = \sqrt{A} - \sqrt{A_0}$ the same linear reconstruction as on A, we get $\Psi_{\bullet\pm}$ and at last we have

$$\sqrt{A_0}_{i+1/2\pm} = \sqrt{A_{i+1/2\pm}} - \Psi_{i+1/2\pm}.$$

Step 2 From variables $U_{\bullet-}$ and $U_{\bullet+}$ we get the following reconstructed variables

$$\begin{cases} \sqrt{A_{i+1/2L}} = \max(\Psi_{i+1/2-} + \min(\sqrt{A_0}_{i+1/2-}, \sqrt{A_0}_{i+1/2+}), 0) \\ U_{i+1/2L} = (A_{i+1/2L}, A_{i+1/2L}u_{i+1/2-})^t \\ \sqrt{A_{i+1/2R}} = \max(\Psi_{i+1/2+} + \min(\sqrt{A_0}_{i+1/2-}, \sqrt{A_0}_{i+1/2+}), 0) \\ U_{i+1/2R} = (A_{i+1/2R}, A_{i+1/2R}u_{i+1/2+})^t \end{cases}. \tag{38}$$

Step 3 In order to get a consistent well-balanced scheme, it is necessary to add a centered source term Fc_i. Scheme (17) becomes

$$U_i^{n+1} = U_i^n - \frac{\Delta t}{\Delta x}\left(F_{i+1/2L}^n - F_{i-1/2R}^n - Fc_i^n\right),$$

where

$$\begin{array}{l} F_{i+1/2L}^n = F_{i+1/2}^n + S_{i+1/2-} \\ F_{i-1/2R}^n = F_{i-1/2}^n + S_{i-1/2+} \end{array},$$

with

$$S_{i+1/2-} = \begin{pmatrix} 0 \\ \mathcal{P}(A_{i+1/2-}^n) - \mathcal{P}(A_{i+1/2L}^n) \end{pmatrix}$$

DOI: 10.1002/fld

$$S_{i-1/2+} = \begin{pmatrix} 0 \\ \mathcal{P}(A^n_{i-1/2+}) - \mathcal{P}(A^n_{i-1/2R}) \end{pmatrix}$$

and

$$Fc_i = \begin{pmatrix} 0 \\ \dfrac{k}{\rho\sqrt{\pi}} \dfrac{(A^n_{i+1/2-})^{3/2} - (A^n_{i-1/2+})^{3/2}}{3} \Delta\sqrt{A_{0i}} \end{pmatrix},$$

with $\Delta\sqrt{A_{0i}} = \sqrt{A_0}_{i+1/2-} - \sqrt{A_0}_{i-1/2+}$. The numerical flux $F^n_{i+1/2}$ is calculated as at first order (3.2.1), *i.e.* with the variables obtained with the hydrostatic reconstruction (38).

Thus we get a second order scheme in space which writes

$$U^{n+1} = U^n + \Delta t \Phi(U^n) \text{ with } U = (U_i)_{i\in\mathbb{Z}}$$

and

$$\Phi(U^n_i) = -\frac{1}{\Delta x}\left(F^n_{i+1/2L} - F^n_{i-1/2R} - Fc^n_i\right). \tag{39}$$

Step 4 The second order in time is recovered by a second order TVD (Total Variation Diminishing) Runge-Kutta (see [81]), namely the Heun method

$$\begin{aligned} \widetilde{U}^{n+1} &= U^n + \Delta t \Phi(U^n), \\ \widetilde{U}^{n+2} &= \widetilde{U}^{n+1} + \Delta t \Phi(\widetilde{U}^{n+1}), \\ U^{n+1} &= \frac{U^n + \widetilde{U}^{n+2}}{2}, \end{aligned} \tag{40}$$

where Φ is defined by (39). This method is a kind of predictor-corrector method.

A more complete modelling of the arterial flow will imply other source terms (diffusion, tension,...). To observe those effects one has to use a higher order scheme, as performed for shallow water in [83] and [72].

4. VALIDATION

4.1. About the chosen examples

The chosen examples are more for sake of illustration of the previous scheme rather than for validation on real clinical datas. So, the extremities of the arteries will be non reflecting and the numerical values are more indicative rather than clinically relevant. Those examples will show that the scheme behaves well and that some validations from linearised or exact solutions may be reobtained. More specifically we insist on the cases with large change of initial section like sudden constriction and sudden expansion. Even we present here an aneurism, flow in a stenosis could also be treated.

4.2. The ideal tourniquet

In the Saint-Venant community, the dam break problem is a classical test case [84] (in compressible gas dynamics, it is referred as the Sod tube, LeVeque [85] or Lighthill [3] or [86]). We have

DOI: 10.1002/fld

an analytical solution of this problem thanks to the characteristic method. So, we consider the analogous of this problem in blood flow: a tourniquet is applied and we remove it instantaneously. Of course, this is done in supposing that the pulsatile effects are neglected, so it is more a test case rather than a real tourniquet. Any way, with the previous hypothesis, we get a Riemann problem. This test allows us to study the ability of the numerical scheme to give the front propagation properly, we notice that the non linear terms are tested (but neither the viscous ones nor the change of basic radius). As we consider an artery with a constant radius at rest and without friction, we consider

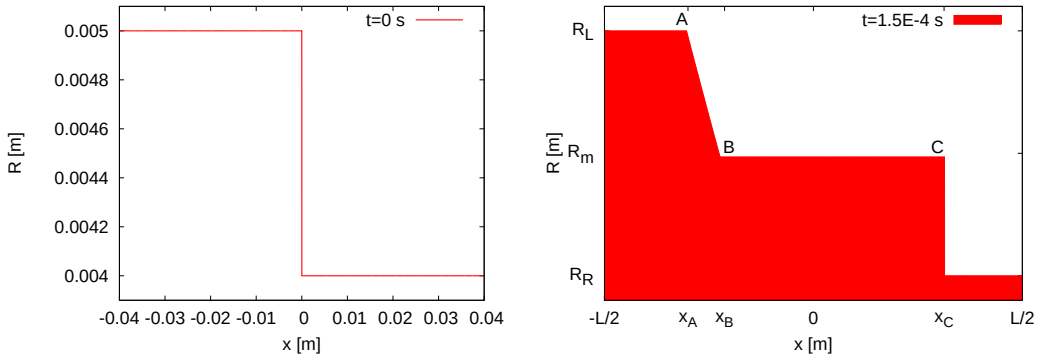

Figure 3. (a) The ideal tourniquet radius initial conditions: a discontinuous initial radius (or pression) is imposed with no velocity (the blood is blocked), (b) analytical solution of the radius at time $t > 0$: a shock wave is moving downstream (to the right) and an expansion wave upstream (to the left).

the system (3) without source term. L is the length of the arteria with $x \in [-L/2, L/2]$. The initial conditions are

$$A(x,0) = \begin{cases} A_L \text{ for } x \leq 0 \\ A_R \text{ for } x > 0 \end{cases}, \tag{41}$$

with $A_L > A_R$ and $Q(x,0) = u(x,0) = 0$ (see figure 3).

As for the dam break, with the characteristic method we get an analytical solution. At time $t > 0$, from the upstream to the downstream of the artery, we have four different states (as illustrated for the radius $R = \sqrt{A/\pi}$ in Figure 3b):

1. Upstream point A located at $x_A(t) = -c_L t$, the state is the same as the initial one:

$$\begin{cases} A(x,t) = A_L \\ u(x,t) = 0 \end{cases}. \tag{42}$$

2. Between point A and point B located at $x_B(t) = (u_M - c_M)t = (4c_L - 5c_M)t$ (the subscript stands for the intermediate state in the following zone), we have

$$\begin{cases} u(x,t) = \dfrac{4}{5}\dfrac{x}{t} + \dfrac{4}{5}c_L \\ \\ c(x,t) = -\dfrac{1}{5}\dfrac{x}{t} + \dfrac{4}{5}c_L \end{cases}. \tag{43}$$

DOI: 10.1002/fld

3. Between point B and C located at $x_C(t) = st$, with the Rankine Hugoniot relation $s = A_M u_M/(A_M - A_R)$. We have an intermediate state

$$\begin{cases} A(x,t) = A_M \\ u(x,t) = u_M \end{cases}, \tag{44}$$

where the variables s, A_M, u_M and $Q_M = u_M A_M$ are obtained thanks to the following system

$$\begin{cases} u_M + 4c_M = u_L + 4c_L \\ Q_R - Q_M = s(A_R - A_M) \\ \left(\frac{Q_R^2}{A_R} + \frac{k}{3\rho\sqrt{\pi}} {A_R}^{3/2}\right) - \left(\frac{Q_M^2}{A_M} + \frac{k}{3\rho\sqrt{\pi}} {A_M}^{3/2}\right) = s(Q_R - Q_M) \end{cases}.$$

As $u_R = u_L = Q_R = Q_L = 0$, this system reduces to

$$\begin{cases} u_M + 4c_M = 4c_L \\ Q_M = s(A_M - A_R) \\ \left(\frac{Q_M^2}{A_M} + \frac{k}{3\rho\sqrt{\pi}} {A_M}^{3/2}\right) - \frac{k}{3\rho\sqrt{\pi}} {A_R}^{3/2} = sQ_M \end{cases}.$$

This system is solved iteratively.

4. Downstream point C, the state is the same as the initial one

$$\begin{cases} A(x,t) = A_R \\ u(x,t) = 0 \end{cases}. \tag{45}$$

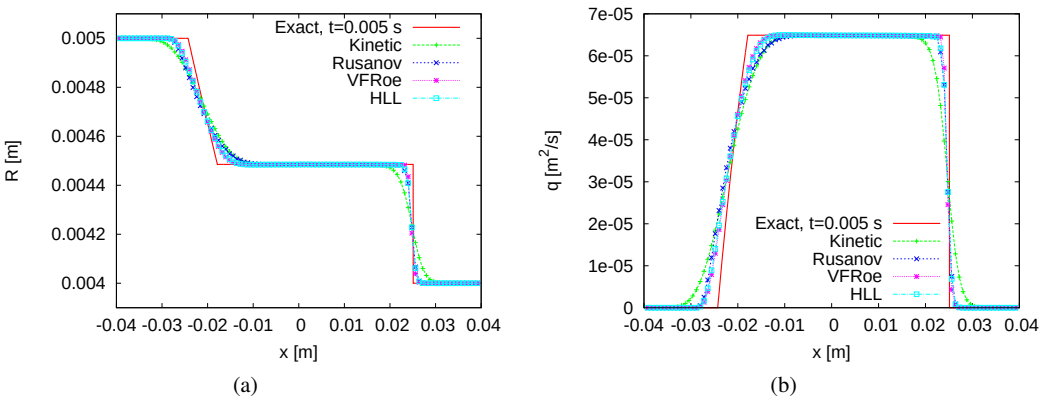

Figure 4. Snapshots of the ideal tourniquet – comparison between analytical and numerical results at $t = T_{end}$: (a) radius and (b) discharge.

The simulations were performed with the first order scheme with each of the fluxes, $J = 100$ cells and a fix CFL of 1 (0.5 for the kinetic flux) and we have used the following numerical values $C_f = 0$, $k = 1.0\ 10^7$Pa/m, $\rho = 1060$m^3, $R_L = 5.\ 10^{-3}$m, $R_R = 4.\ 10^{-3}$m, $L = 0.08$m, $T_{end} = 0.005$s, $c_R = \sqrt{kR_R/(2\rho)} \simeq 4.34$m/s, $c_L = \sqrt{kR_L/(2\rho)} \simeq 4.86$m/s. An initial flow at rest: $Q(x, t = 0) =$

DOI: 10.1002/fld

$0\mathrm{m}^3/\mathrm{s}$ and

$$A(x, t = 0) = \begin{cases} \pi {R_L}^2, \text{ if } x \in [-0,04 : 0] \\ \pi {R_R}^2, \text{ if } x \in]0 : 0,04] \end{cases}.$$

As illustrated in Figure 4, we notice that the Rusanov and Kinetic fluxes are more diffusive than the others. With mesh refinement and/or scheme order increasing, we should improve the results both at the shock level and the expansion wave. As noticed in [75] for the shallow water equations, the VFRoe-ncv needs more cpu time than the HLL flux. So in what follows we will focus on the HLL flux. This is a rather severe test case as in practice, $|Q/(Ac)|$ is less than 10 % in physicological cases.

4.3. Wave equation

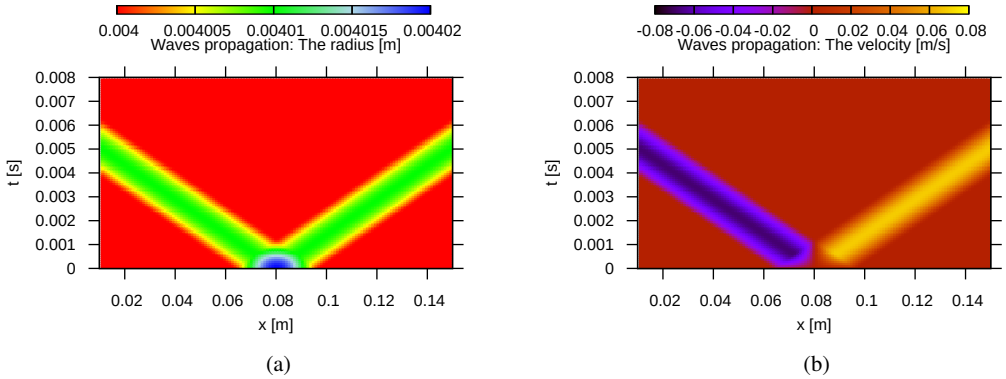

Figure 5. The propagation of an initial (non physiological) pulse given at $t = 0$ in space and time: (a) radius and (b) velocity: the initial perturbation splits into a forward and backward travelling wave (colors online).

So, as in practice, in arteries, the mean velocity is far smaller than the Moens Korteweg celerity $|Q/(Ac)| \ll 1$, here we will study the ability to catch the relevant small linearised wave propagation speeds. We look at the evolution of a given perturbation of radius with no velocity perturbation and see how it evolves. Thus we consider the system without friction, with a constant section at rest, a steady state $(R_0, u_0 = 0)$. Looking at perturbation at a small level $\varepsilon \ll 1$, we have $(R, u) = (R_0 + \varepsilon R_1, \varepsilon u_1)$ where subscript 1 refers to the perturbation. Substitution in (3) and neglecting the small terms, it becomes the d'Alembert equation for the perturbations u_1 and R_1:

$$\partial_t^2(u_1, R_1) - {c_0}^2 \partial_x^2(u_1, R_1) = 0, \tag{46}$$

the same is valid for variables $Q_1 = A_0 u_1$ the perturbation of flux and $p_1 = kR_1$ the perturbation of pressure with the Moens Korteweg wave velocity

$$c_0 = \sqrt{\frac{k\sqrt{A_0}}{2\rho\sqrt{\pi}}} = \sqrt{\frac{kR_0}{2\rho}}. \tag{47}$$

Prepared using fldauth.cls
DOI: 10.1002/fld

With initial conditions $u_1(x,0)=0$, $R_1(x,0)=\phi(x)$ we obtain so analytical solution:

$$\begin{cases} R(x,t) = R_0 + \dfrac{\varepsilon}{2}\left[\phi\left(x-c_0t\right)+\phi\left(x+c_0t\right)\right] \\ u(x,t) = -\dfrac{\varepsilon}{2}\dfrac{c_0}{R_0}\left[-\phi\left(x-c_0t\right)+\phi\left(x+c_0t\right)\right] \end{cases}.$$

The following numerical values have been used for the figure 5: $J=200$, $C_f=0$, $k=1.0\ 10^8$Pa/m, $\rho=1060\text{m}^3$, $R_0=4.\ 10^{-3}$m, $L=0.16$m, $T_{end}=0.008$s, $c_0=\sqrt{kR_0/(2\rho)}\simeq 13.7$m/s. As initial conditions, we take a fluid at rest $Q(x,0)=0\text{m}^3/\text{s}$ with an initial deformation of the radius

$$A(x,0)=\begin{cases} \pi {R_0}^2, \text{ if } x\in[0:40L/100]\cup[60L/100:L] \\ \pi {R_0}^2\left[1+\varepsilon\sin\left(\pi\dfrac{x-40L/100}{20L/100}\right)\right]^2, \text{ if } x\in]40L/100:60L/100[\end{cases},$$

with $\varepsilon=5.10^{-3}$. As illustrated, in Figure 6a, we get two waves, propagating on the right (respectively left) with a positive (resp. negative) velocity. The two waves are represented at several moments. We notice no numerical diffusion.

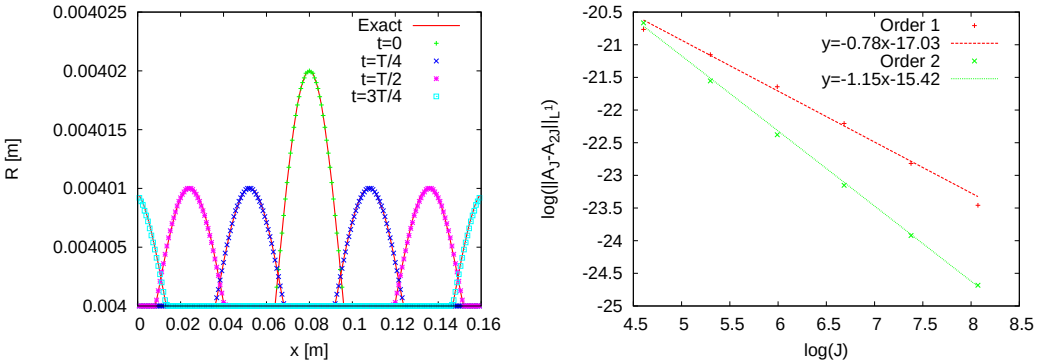

(a) (b)

Figure 6. (a) Radius as function of the position at 3 time steps: $t=0$, $t=T_{end}/4$, $t=T_{end}/2$ and $t=3T_{end}/4$, comparison between the first order scheme with HLL flux and exact solution and (b) the error made on the area calculation at $t=0.004s$.

4.4. "The man at eternal rest"

The previous test case did not involve drastic changes in the basic radius. We will show in this section that a not adapted source term treatment in (3) may give non-physical velocity. In this test case, we consider a configuration with no flow and with a change of radius $R_0(x)$, this is the case for a dead man with an aneurism. Thus the section of the artery is not constant and the velocity is $u(x,t)=0$ m/s. We use the following numerical values. $J=50$ cells, $C_f=0$, $k=1.0\ 10^8$Pa/m, $\rho=1060\text{m}^3$, $L=0.14$m, $T_{end}=5$s. As initial conditions, we take a fluid at rest $Q(x,0)=0\text{m}^3/\text{s}$

Prepared using fldauth.cls
DOI: 10.1002/fld

and

$$R(x,0) = R_0(x) = \begin{cases} R_o \text{ if } x \in [0 : x_1] \cup [x_4 : L] \\ R_o + \dfrac{\Delta R}{2}\left[\sin\left(\left(\dfrac{x-x_1}{x_2-x_1}\pi - \pi/2\right)\right) + 1\right], \text{ if } x \in]x_1 : x_2[\\ R_o + \Delta R \text{ if } x \in [x_2 : x_3] \\ R_o + \dfrac{\Delta R}{2}\left(\cos\left(\dfrac{x-x_3}{x_4-x_3}\pi\right) + 1\right), \text{ if } x \in]x_3 : x_4[\end{cases},$$

with $R_o = 4.0\ 10^{-3}$m, $\Delta R = 1.0\ 10^{-3}$m, $x_1 = 1.0\ 10^{-2}$m, $x_2 = 3.05\ 10^{-2}$m, $x_3 = 4.95\ 10^{-2}$m and $x_4 = 7.0\ 10^{-2}$m (figure 7a).

As illustrated in Figure 7b, with an explicit treatment of the source term in A_0, we get non zero velocities at the arteria cross section variation level. The "man at eternal rest" is not preserved, spurious flow appear (avoiding artifacts such as [87]). As expected, the hydrostatic reconstruction (21) preserves exactly the steady state at rest.

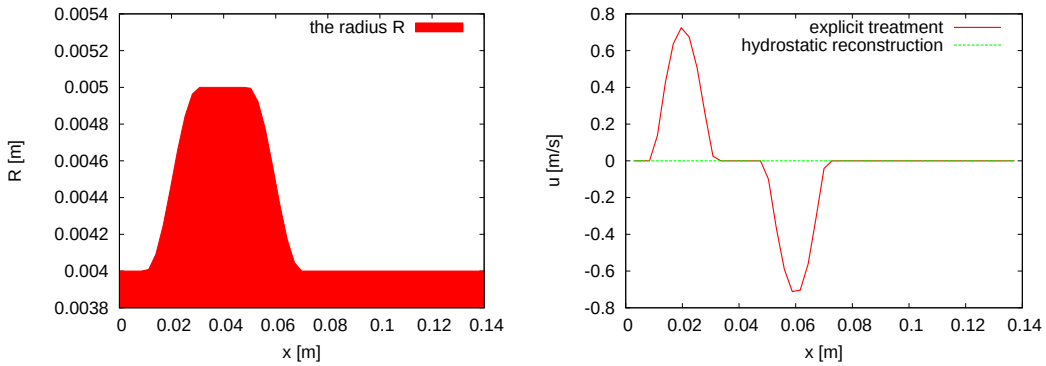

(a) (b)

Figure 7. The "dead man case": (a) the radius of the arteria, (b) comparison of the velocity at time $t = 5$s between an explicit treatment of the source term and the hydrostatic reconstruction. The spurious flow effect is clearly visible if an inappropriate scheme is chosen.

4.5. Wave reflection-transmission in an aneurism

4.5.1. Analytical linear transmission We observed that waves propagate fairly well in a straight tube, we now observe the reflexion and transmission trough a sudden change of section (from A_L to A_R) in an elastic tube. The d'Alembert equation (46) admits harmonic waves $e^{i(\omega t - x/c_0)}$, so that a plane wave is (symbol 1 represents a linear perturbation as in section 4.3):

$$Q_1 = Y_0 p_1, \text{ with } p_1 \propto \mathcal{R}e(e^{i(\omega t - x/c_0)})$$

and $Y_0 = A_0/(\rho c_0)$ is called the characteristic admittance. With this definition, we can look at a change of section from a radius R_L to a radius R_R: an imposed right traveling plane wave $e^{i(\omega t - x/c_L)}$ moving at celerity c_L in the left media (subscript L) will experience a transmission in the right media (subscript R) (and will move at celerity c_R) and a reflexion (and move at celerity $-c_L$). The coefficients of transmission and reflexion depend on the two admittances of the two

DOI: 10.1002/fld

media L and R (see Lighthill or Pedley):

$$Tr = \frac{2Y_L}{Y_L + Y_R} \text{ and } Re = \frac{Y_L - Y_R}{Y_L + Y_R}.$$

As the admittance does not depend on the frenquency ω, any signal (by Fourier decomposition) will be transmitted and reflected with those values.

Here we will study the reflection and the transmission of a small wave in an aneurism.

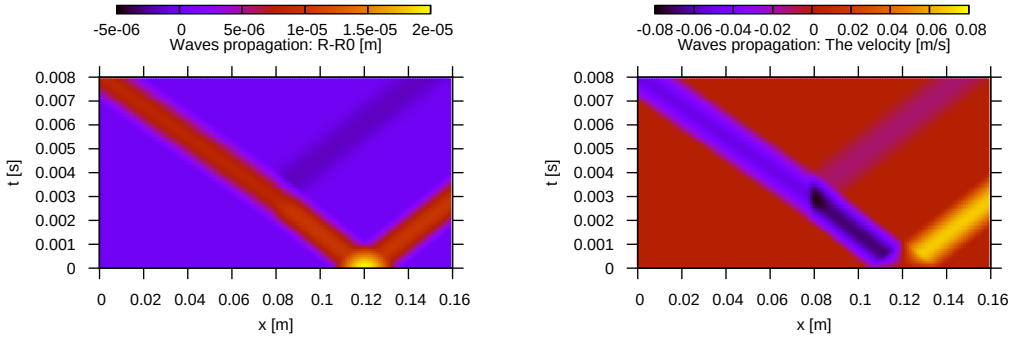

(a) (b)

Figure 8. To an expansion, the propagation of an initial pulse in space and time: (a) radius and (b) velocity (colors online).

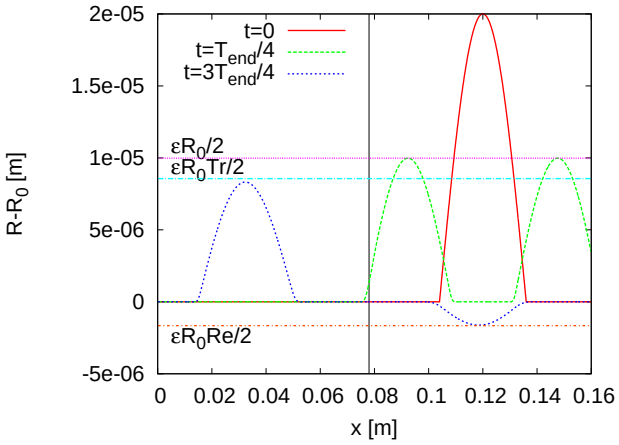

Figure 9. Radius as function of the position at 3 time steps: $t = 0$, $t = T_{end}/4$, $t = T_{end}/2$ and $t = 3T_{end}/4$. The dotted lines represent the level of the predicted reflexion (Re) and transmission (Tr) coefficients.

4.5.2. Propagation of a pulse to and from an expansion First we test the case of a pulse in a section R_R passing trough an expansion: $A_L > A_R$, taking the following numerical values: $J = 1500$ cells, $C_f = 0$, $k = 1.0\ 10^8$Pa/m, $\rho = 1060$m^3, $R_L = 5.\ 10^{-3}$m, $R_R = 4.\ 10^{-3}$m, $\Delta R = 1.0\ 10^{-3}$m, $L = 0.16$m, $T_{end} = 8.0\ 10^{-3}$s, $c_L = \sqrt{kR_L/(2\rho)} \simeq 15.36$m/s and $c_R = \sqrt{kR_R/(2\rho)} \simeq 13.74$m/s. We

DOI: 10.1002/fld

take a decreasing shape on a rather small scale:

$$R_0(x) = \begin{cases} R_R + \Delta R = R_b & \text{if } x \in [0 : x_1] \\ R_R + \dfrac{\Delta R}{2}\left[1 + \cos\left(\dfrac{x - x_1}{x_2 - x_1}\pi\right)\right] & \text{if } x \in]x_1 : x_2] \\ R_R & \text{else} \end{cases}, \tag{48}$$

with $x_1 = 19L/40$ and $x_2 = L/2$. As initial conditions, we consider a fluid at rest $Q(x,0) = 0\text{m}^3/\text{s}$ and the following perturbation of radius:

$$R(x,0) = \begin{cases} R_0(x)\left[1 + \varepsilon \sin\left(\dfrac{100}{20L}\pi\left(x - \dfrac{65L}{100}\right)\right)\right] & \text{if } x \in [65L/100 : 85L/100] \\ R_0(x) & \text{else} \end{cases},$$

with $\varepsilon = 5.0\ 10^{-3}$.

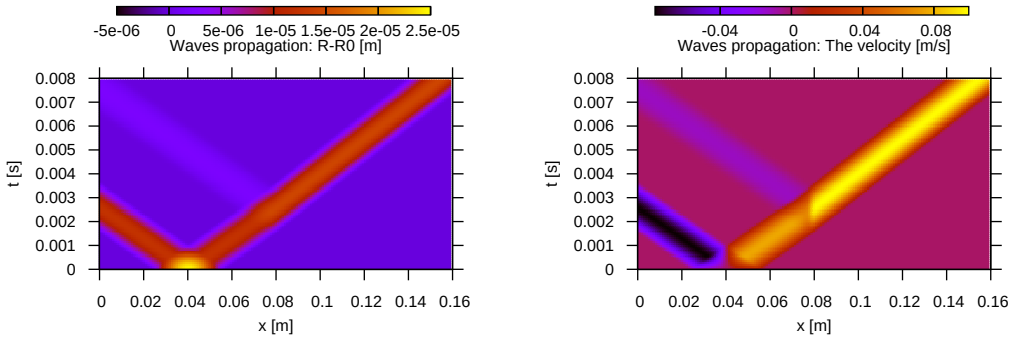

(a) (b)

Figure 10. From an expansion, the propagation of an initial pulse in space and time: (a) radius and (b) velocity (colors online).

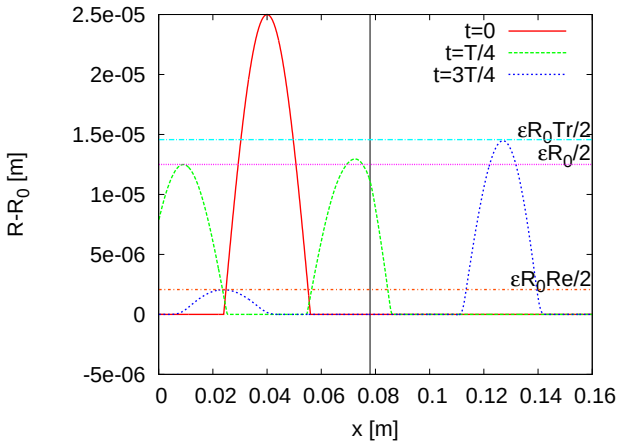

Figure 11. Radius as function of the position at 3 time steps: $t = 0$, $t = T_{end}/4$, $t = T_{end}/2$ and $t = 3T_{end}/4$. The dotted lines represent the level of the predicted reflexion (Re) and transmission (Tr) coefficients.

DOI: 10.1002/fld

Results showing the wave propagation and expansion are in Figure 8. In Figure 9 we have the amplitude of the pulse before and after the change of section, the level of the analytical prediction of T and R is plotted as well showing that the levels are preserved.

The same is done for a pulse propagating from an expansion. So, just the radius is changed:

$$R(x,0) = \begin{cases} R_0(x)\left[1+\varepsilon\sin\left(\dfrac{100}{20L}\pi\left(x-\dfrac{15L}{100}\right)\right)\right] & \text{if } x\in[15L/100:35L/100] \\ R_0(x) & \text{else} \end{cases},$$

with $\varepsilon = 5.0\ 10^{-3}$. Similar results showing the wave propagation are in Figure 10a and 10b. In Figure 11 the amplitude of the pulse corresponds to the level predicted by the analytical linearised solution.

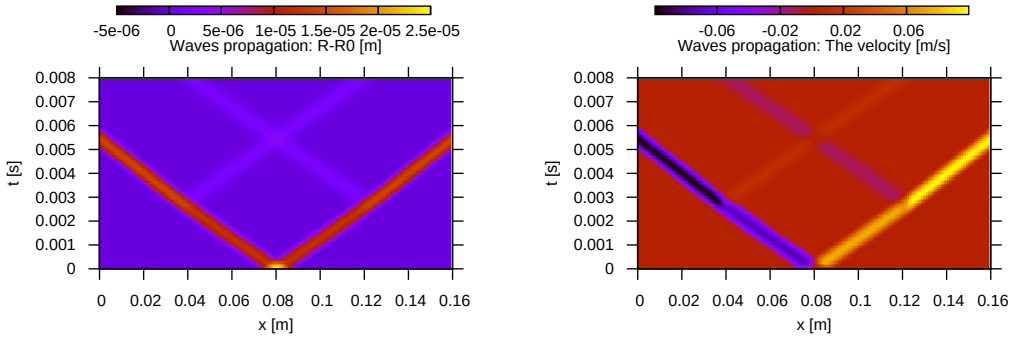

(a) (b)

Figure 12. The propagation in an aneurysm of an initial pulse in space and time: (a) radius and (b) velocity. We note the expected reflexions at the position where the vessel changes his shape (colors online).

4.5.3. The aneurism In this part we put an expansion and one constriction modelling an aneurism. An initial pulse at the center C of this aneurism propagates in the right and left direction to the boundaries B. One sees in Figure 12 the reflexions and transmissions at the position of the variation of radius. These plots have been done with the following numerical values: $J = 1500$ cells, $C_f = 0$, $k = 1.0\ 10^8$Pa/m, $\rho = 1060$m^3, $R_B = 4.\ 10^{-3}$m, $R_C = 5.\ 10^{-3}$m, $\Delta R = 1.0\ 10^{-3}$m, $L = 0.16$m, $T_{end} = 8.0\ 10^{-3}$s, $c_B = \sqrt{kR_B/(2\rho)} \simeq 13.74$m/s and $c_C = \sqrt{kR_C/(2\rho)} \simeq 15.36$m/s. With the given shape

$$R_0(x) = \begin{cases} R_B & \text{if } x\in[0:x_1]\bigcup[x_4:L] \\ R_B + \dfrac{\Delta R}{2}\left[1-\cos\left(\dfrac{x-x_1}{x_2-x_1}\pi\right)\right] & \text{if } x\in]x_1:x_2] \\ R_B+\Delta R = R_C & \text{if } x\in]x_2:x_3] \\ R_B + \dfrac{\Delta R}{2}\left[1+\cos\left(\dfrac{x-x_3}{x_4-x_3}\pi\right)\right] & \text{if } x\in]x_3:x_4[\end{cases}, \quad (49)$$

DOI: 10.1002/fld

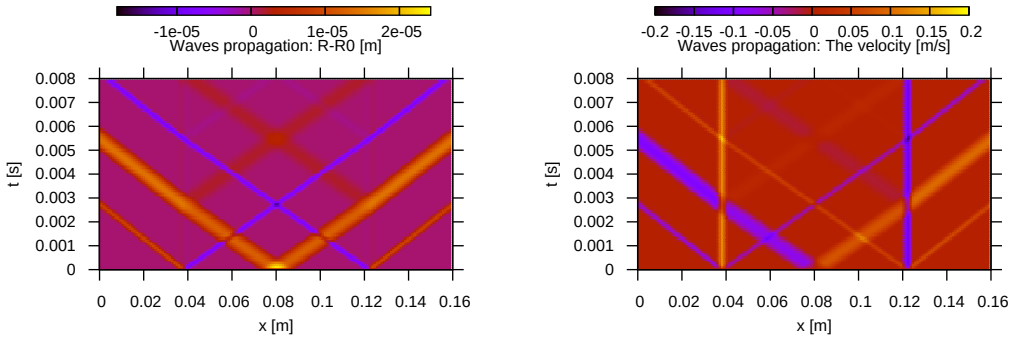

(a) (b)

Figure 13. A scheme which does not preserve the "man at eternal rest" generates spurious waves were the radius changes (colors online).

with $x_1 = 9L/40$, $x_2 = L/4$, $x_3 = 3L/4$ and $x_4 = 31L/40$. As initial conditions, we consider a fluid at rest $Q(x,0) = 0\text{m}^3/\text{s}$ and the initial perturbation:

$$R(x,0) = \begin{cases} R_0(x)\left[1 + \varepsilon \sin\left(\frac{100}{10L}\pi\left(x - \frac{45L}{100}\right)\right)\right] & \text{if } x \in [45L/100 : 55L/100] \\ R_0(x) & \text{else} \end{cases},$$

with $\varepsilon = 5.0\ 10^{-3}$.

4.5.4. Non adapted treatment of the source terms To insist on the adapted treatment of the source terms, we present in this sub section what happens if a naive scheme is taken like in subsection 3.2.1. We clearly see in Figure 13 that at the change of radius reflected and spurious wave appear. The previous constant velocities are present like in Figure 13b. Furthermore, the initial data give traveling waves coming from the position of the change of section. This clearly shows the influence of the source terms in the discretization.

4.6. Wave "damping"

In this last test case, we look at the viscous damping term in the linearized momentum equation. This is the analogous of the Womersley [88] problem, we consider a periodic signal at the inflow which is a perturbation of a steady state ($R_0 = Cst, u_0 = 0$) with a constant section at rest. We consider the set of equations 3 with the friction term under the nonconservative form with the variables (R, u), this system writes

$$\begin{cases} \partial_t R + u\partial_x R + \dfrac{R}{2}\partial_x u = 0 \\ \partial_t u + u\partial_x u + \dfrac{k}{\rho}\partial_x R = -\dfrac{C_f}{\pi}\dfrac{u}{R^2} \end{cases}.$$

DOI: 10.1002/fld

We take $R = R_0 + \varepsilon R_1$ and $u = 0 + \varepsilon u_1$, where (R_1, u_1) is the perturbation of the steady state. We have after linearisation of the equations:

$$\begin{cases} 2\partial_t R_1 + R_0 \partial_x u_1 = 0 \\ \partial_t u_1 + \dfrac{k}{\rho}\partial_x R_1 = -\dfrac{C_f}{\pi}\dfrac{u_1}{{R_0}^2} \end{cases},$$

which may be combined in two wave equations with source term

$$\partial_t^2(u_1, R_1) - {c_0}^2 \partial_x^2(u_1, R_1) = -\frac{C_f}{\pi}\frac{\partial_t(u_1, R_1)}{{R_0}^2}. \tag{50}$$

Looking for progressive waves (*i.e.* under the form $e^{i(\omega t - Kx)}$), we obtain the dispersion relation

$$K^2 = \frac{\omega^2}{{c_0}^2} - i\frac{\omega C_f}{\pi R_0 {c_0}^2}, \tag{51}$$

with $\omega = 2\pi/T_{pulse}$, T_{pulse} the time length of a pulse and $K = k_r + ik_i$, the wave vector not to be confused with the stiffness,

$$\begin{cases} k_r = \left[\dfrac{\omega^4}{{c_0}^4} + \left(\dfrac{\omega C_f}{\pi {R_0}^2 {c_0}^2}\right)^2\right]^{1/4} \cos\left(\dfrac{1}{2}\arctan\left(-\dfrac{C_f}{\pi {R_0}^2 \omega}\right)\right) \\ k_i = \left[\dfrac{\omega^4}{{c_0}^4} + \left(\dfrac{\omega C_f}{\pi {R_0}^2 {c_0}^2}\right)^2\right]^{1/4} \sin\left(\dfrac{1}{2}\arctan\left(-\dfrac{C_f}{\pi {R_0}^2 \omega}\right)\right) \end{cases}. \tag{52}$$

For the numerical applications, we impose the incoming discharge

$$Q_b(t) = Q_{amp}\sin(\omega t)\mathrm{m}^3/\mathrm{s},$$

with Q_{amp} the amplitude of the inflow discharge. We get a damping wave in the domain

$$Q(t,x) = \begin{cases} 0 & , \text{ if } k_r x > \omega t \\ Q_{amp}\sin\left(\omega t - k_r x\right) e^{k_i x} & , \text{ if } k_r x \leq \omega t \end{cases}, \tag{53}$$

where $Q_b(t)$ is the discharge imposed at $x = 0$.

The following numerical values allow to plot figure 14a to 14d. For C_f, we took 4 different values ($C_f = 0$, $C_f = 0.000022$, $C_f = 0.000202$ and $C_f = 0.005053$, corresponding to Womersley parameters $\alpha = \infty$, $\alpha = 15.15$, $\alpha = 5$ and $\alpha = 1$), $J = 50$, 100, 200, 400, 800 cells, $k = 1.10^8$Pa/m, $\rho = 1060\mathrm{m}^3$, $R_0 = 4.10^{-3}$m, $L = 3$m, $T_{end} = 25$.s. As initial conditions, we take a fluid at rest $Q(x, 0) = 0\mathrm{m}^3/\mathrm{s}$ and as input boundary condition

$$Q_b(t) = Q_{amp}\sin(\omega t)\mathrm{m}^3/\mathrm{s}.$$

with $\omega = 2\pi/T_{pulse} = 2\pi/0.5$s and $Q_{amp} = 3.45.10^{-7}\mathrm{m}^3/\mathrm{s}$. As the flow is subcritical,the discharge is imposed at the outflow boundary thanks to (53) with $x = L$.

In this part, we insist on the comparison between first order and second order. So, we compare first order (HHL1) and second order scheme with both MUSCL (HLL MUSCL) and ENO (HLL ENO)

DOI: 10.1002/fld

$C_f = 0.000022$	HLL1-SI		HLL1-AT		HLL MUSCL-SI		HLL ENO-SI		HLL MUSCL-AT	
J	$\|\|Q - Q_{ex}\|\|_{L^1}$	t_{cpu} [s]	$\|\|Q - Q_{ex}\|\|_{L^1}$	t_{cpu} [s]	$\|\|Q - Q_{ex}\|\|_{L^1}$	t_{cpu} [s]	$\|\|Q - Q_{ex}\|\|_{L^1}$	t_{cpu} [s]	$\|\|Q - Q_{ex}\|\|_{L^1}$	t_{cpu} [s]
50	0.311E-7	0.49	0.309E-7	0.51	0.753E-8	2.7	0.796E-8	2.52	0.753E-8	2.9
100	0.158E-7	1.95	0.157E-7	2	0.232E-8	10.65	0.216E-8	9.95	0.232E-8	11.47
200	0.789E-8	7.8	0.783E-8	7.96	0.121E-8	41.95	0.129E-8	39.3	0.121E-8	45.31
400	0.386E-8	31.26	0.383E-8	31.75	0.458E-9	167.16	0.651E-9	156.47	0.457E-9	179.4
800	0.183E-8	126.06	0.182E-8	126.92	0.267E-9	665.91	0.401E-9	625.62	0.267E-9	717.64
Regression	y=-1.02x-13.27		y=-1.02x-13.27		y=-1.2x-14.19		y=-1.04x-14.86		y=-1.2x-14.19	

$C_f = 0.000202$	HLL1-SI		HLL1-AT		HLL MUSCL-SI		HLL ENO-SI		HLL MUSCL-AT	
J	$\|\|Q - Q_{ex}\|\|_{L^1}$	t_{cpu} [s]	$\|\|Q - Q_{ex}\|\|_{L^1}$	t_{cpu} [s]	$\|\|Q - Q_{ex}\|\|_{L^1}$	t_{cpu} [s]	$\|\|Q - Q_{ex}\|\|_{L^1}$	t_{cpu} [s]	$\|\|Q - Q_{ex}\|\|_{L^1}$	t_{cpu} [s]
50	0.269E-7	0.49	0.311E-7	0.51	0.426E-8	2.63	0.557E-8	2.74	0.513E-8	2.81
100	0.138E-7	1.97	0.157E-7	2	0.181E-8	10.5	0.197E-8	10.89	0.18E-8	11.23
200	0.707E-8	7.85	0.795E-8	7.97	0.984E-9	41.89	0.899E-9	43.46	0.748E-9	44.77
400	0.365E-8	31.23	0.407E-8	31.84	0.505E-9	167.18	0.499E-9	173.43	0.425E-9	180.52
800	0.192E-8	124.92	0.212E-8	127.31	0.283E-9	670.25	0.327E-9	694.69	0.296E-9	718.3
Regression	y=-0.95x-13.7		y=-0.97x-13.5		y=-1.02x-15.24		y=-1.02x-15.2		y=-1.03x-15.29	

$C_f = 0.005053$	HLL1-SI		HLL1-AT		HLL MUSCL-SI		HLL ENO-SI		HLL MUSCL-AT	
J	$\|\|Q - Q_{ex}\|\|_{L^1}$	t_{cpu} [s]	$\|\|Q - Q_{ex}\|\|_{L^1}$	t_{cpu} [s]	$\|\|Q - Q_{ex}\|\|_{L^1}$	t_{cpu} [s]	$\|\|Q - Q_{ex}\|\|_{L^1}$	t_{cpu} [s]	$\|\|Q - Q_{ex}\|\|_{L^1}$	t_{cpu} [s]
50	0.26E-7	0.51	0.396E-7	0.52	0.162E-7	2.68	0.159E-7	2.79	0.334E-7	2.81
100	0.146E-7	1.98	0.215E-7	2.03	0.916E-8	10.56	0.899E-8	11.03	0.176E-7	11.2
200	0.79E-8	7.88	0.112E-7	8.01	0.494E-8	41.94	0.486E-8	43.71	0.907E-8	44.69
400	0.411E-8	31.32	0.576E-8	31.9	0.257E-8	167.32	0.253E-8	174.25	0.46E-8	178.64
800	0.21E-8	125.15	0.291E-8	127.18	0.131E-8	669.56	0.129E-8	693.64	0.231E-8	714.29
Regression	y=-0.91x-13.9		y=-0.94x-13.33		y=-0.91x-14.34		y=-0.91x-14.36		y=-0.96x-13.43	

Table I. The wave "damping": L^1 errors on the discharge Q and CPU times t_{cpu} for $C_f = 0.000022$, 0.000202 and 0.005053. (AT) apparent topgraphy, (SI) semi-implicit and (HLL1) first order scheme with HLL flux.

DOI: 10.1002/fld

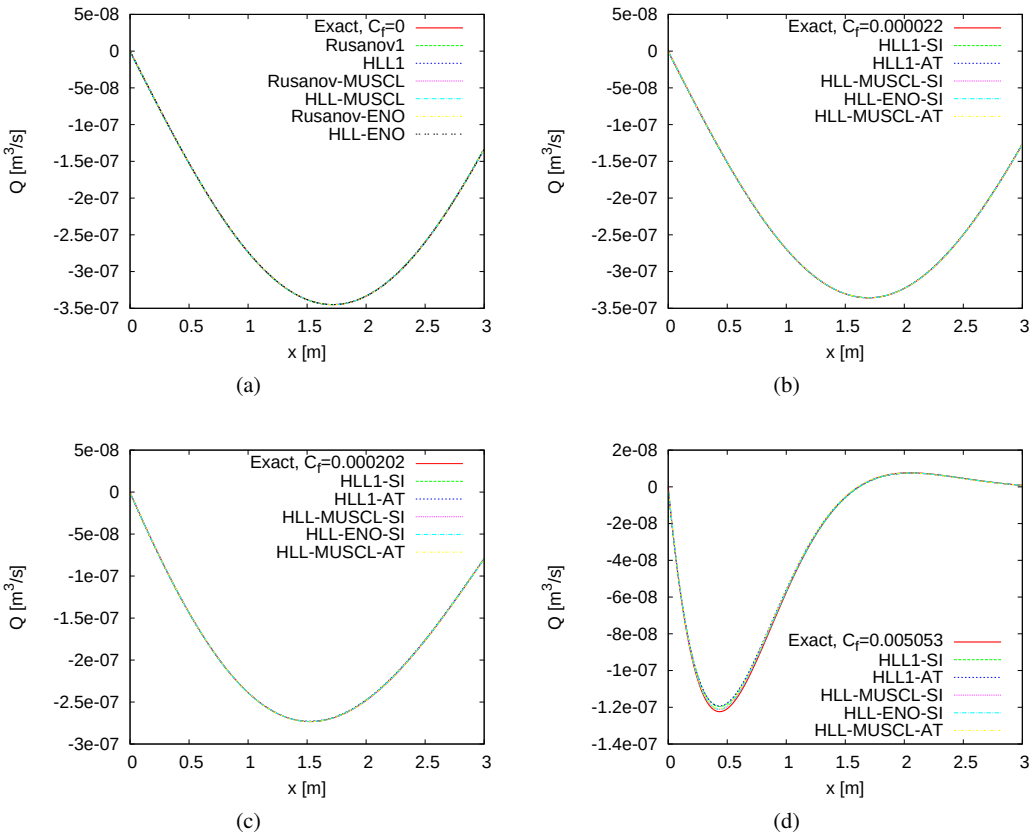

Figure 14. The damping of a discharge wave (a) $C_f = 0$, $\alpha = \infty$, (b) $C_f = 0.000022$, $\alpha = 15.15$, (c) $C_f = 0.000202$, $\alpha = 5$ and (d) $C_f = 0.005053$, $\alpha = 1$. The friction has been treated with either the semi-implicit method (SI) or the apparent topography method (AT) and $J = 800$.

linear reconstruction. When C_f is not null, semi-implicit (SI) and apparent topography (AT) are compared. We should remark that as the friction increases the structure of the system (1) changes and goes from a transport/ wave behavior to a diffusive behavior. The diffusive behavior comes from the fact that as C_f increases, finally the momentum equation contains at leading order only the friction term and the elastic one: $C_f Q_1/A_0 \sim -(A_0 k/\rho)\partial_x R$ and so, using the conservation of mass:

$$\frac{\partial R}{\partial t} = D\frac{\partial^2 R}{\partial x^2} \text{ with } D = \frac{k\pi R_0^2}{2\rho C_f},$$

which is consistent with (51) at small ω. However solving a "heat equation" with a "wave technique" seems to be adapted. Indeed, we notice a fair agreement between the numerics and the analytical solution in Figures 14a to 14d. "Errors made" between numerical results and the exact solution of the linearized system are given for information with CPU time in tables I and II.

4.7. Discussion on numerical precision

Indeed, the notion of scheme order fully depends on the regularity of the solution. Moreover, calculating the error on the solution of the linearized system does not provide information from

DOI: 10.1002/fld

a numerical point of view (sections 4.3 and 4.6). Our purpose is not to verify the second order accuracy of the numerical method (it has already been verified for the Shallow Water applications in [48, 74, 78]). But these errors computations allow us to verify that for these configurations the nonlinear system has a linear behavior. And this linear behavior is perfectly captured by the scheme and the physical model. Precision is increased by increasing the order of the numerical method (as shown on Figure 6b and as illustrated in tables I and II). The theoretical order of the schemes is not recovered for the wave test in section 4.3 (0.78 instead of 1 and 1.15 instead of 2) this is due to the regularity of the solution of the initial system. Indeed, this solution is only continuous. In addition, the system has no term of order 2, then the interest in using a second order method is to save computing time for a given accuracy (see Figure 15). The semi-implicit treatment and the apparent topography give closed results. However, when friction increases ($C_f = 0.005053$), the semi-implicit method is closer to the linearised solution.

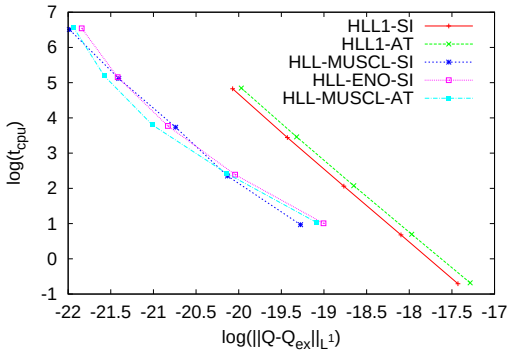

Figure 15. The wave "damping": The efficiency curves for $C_f = 0.000202$.

$C_f = 0$	HLL1		HLL MUSCL		HLL ENO	
J	$\|\|Q - Q_{ex}\|\|_{L^1}$	t_{cpu} [s]	$\|\|Q - Q_{ex}\|\|_{L^1}$	t_{cpu} [s]	$\|\|Q - Q_{ex}\|\|_{L^1}$	t_{cpu} [s]
50	0.314E-7	0.49	0.104E-7	2.63	0.11E-7	2.7
100	0.159E-7	1.93	0.508E-8	10.49	0.546E-8	10.7
200	0.801E-8	7.7	0.238E-8	40.93	0.263E-8	42.6
400	0.397E-8	30.93	0.103E-8	163.47	0.118E-8	170.32
800	0.192E-8	123.28	0.36E-9	654.64	0.433E-9	681.26
Regression	y=-1.007x-13.32		y=-1.2x-13.59		y=-1.155x-13.72	

Table II. The wave "damping": L^1 errors on the discharge Q and CPU times t_{cpu} for $C_f = 0$.

5. CONCLUSION

In this paper we have considered the classical 1-D model of flow in an artery, we have presented a new numerical scheme and some numerical tests. The new proposed scheme has been obtained in following recent advances in the shallow-water Saint-Venant community. This community has been confronted to spurious flows induced by the change of topography in not well written schemes. In blood-flows, it corresponds to the treatment of the terms due to a variating initial shape of the artery,

DOI: 10.1002/fld

which arises is stenosis, aneurisms, or taper. To write the method, we have insisted on the fact that the effective conservative variables are: the artery area A and the discharge Q, which was not clearly observed up to now. The obtained conservative system has been then discretized in order to use the property of equilibrium of "the man at eternal rest" analogous to the "lake at rest" in Saint-Venant equations. If this property is not preserved in the numerical stencil, spurious currents arise in the case of a variating vessel. For sake of illustration, if the terms are treated in a too simple way, we have exhibited a case with an aneurism which induces a non zero flux of blood Q. In a pulsatile case, the same configuration creates extra waves as well. An analogous of dam break (here a tourniquet) was used to validate the other terms of the dicretisation. Other less demanding examples have been performed: linear waves without and with damping in straight tubes. Good behaviour is obtained in those pertinent test cases that explore all the parts of the equations.

The well-balanced finite volume scheme that we propose preserves the volume of blood and avoids non physical case behavior. Thus we get a stable scheme and the accuracy is improved thanks to a second order reconstruction. The numerical method has been tested on examples which are more "gedanken" than physiological. This means that we only did a first necessary step. The next one is now to test more complex cases such as bifurcations, special boundary conditions and so on, in order to confront and fit to real practical clinical cases one of them being the case of aneurisms, in which as well we can introduce a source term in the mass equation in the case of leaks, we conclude that to look at those difficult problems, a careful treatment of the numerical scheme is important.

We thank ENDOCOM ANR for financial support, we thank Marie-Odile Bristeau and Christophe Berthon for fruitful discussions.

REFERENCES

1. Xiu D, Sherwin SJ. Parametric uncertainty analysis of pulse wave propagation in a model of a human arterial network. *Journal of Computational Physics* 2007; **226**:1385–1407.
2. Parker KH. A brief history of arterial wave mechanics. *Med Biol Eng Comput* Feb 2009; **47**:111–118.
3. Lighthill J. *Waves in Fluids*. 1978.
4. Pedley TJ. *The Fluid Mechanics of Large Blood Vessel*. 1980.
5. Van Steenhoven AA, Van Dongen MEH. Model studies of the aortic pressure rise just after valve closure. *J. Fluid. Mech.* 1986; **166**:93–113.
6. Zagzoule M, Marc-Vergnes JP. A global mathematical model of the cerebral circulation in man. *J. Biomechanics* 1986; **19**(12):1015–1022.
7. Stergiopulos N, Young DF, Rogge TR. Computer simulation of arterial flow with applications to arterial and aortic stenoses. *J. Biomechanics* 1992; **25**(12):1477–1488.
8. Olufsen MS. Structured tree outflow condition for blood flow in larger systemic arteries. *American Journal of Physiology – Heart and Circulatory Physiology* 1999; **276**:257–268.
9. Lagrée PY, Rossi M. Etude de l'écoulement du sang dans les artères: effets nonlinéaires et dissipatifs. *C. R. Acad. Sci. Paris, t322, Série II b* 1996; 401–408.
10. Lagrée PY. An inverse technique to deduce the elasticity of a large artery. *The European Physical Journal* 2000; **9**:153–163.
11. Sherwin SJ, Formaggia L, Peiró J, Franke V. Computational modelling of 1d blood flow with variable mechanical properties and its application to the simulation of wave propagation in the human arterial system. *International Journal for Numerical Methods in Fluids* 2003; **43**:673–700, doi:10.1002/fld.543.
12. Fernández MA, Milišić V, Quarteroni A. Analysis of a geometrical multiscale blood flow model based on the coupling of ode's and hyperbolic pde's. *Technical Report 5127*, INRIA Feb 2004.

DOI: 10.1002/fld

13. Wibmer M. One-dimensional simulation of arterial blood flow with applications. PhD Thesis, eingereicht an der Technischen Universitat Wien – Fakultat fur Technische Naturwissenschaften und Informatik Jan 2004.
14. Martin V, Clément F, Decoene A, Gerbeau JF. Parameter identification for a one-dimensional blood flow model. *ESAIM: PROCEEDINGS*, vol. 14, Gerbeau ECJF (ed.), 2005; 174–200, doi:10.1051/proc:2005014.
15. Formaggia L, Lamponi D, Tuveri M, Veneziani A. Numerical modeling of 1d arterial networks coupled with a lumped parameters description of the heart. *Computer Methods in Biomechanics and Biomedical Engineering* 2006; **9**:273–288.
16. Cavallini N, Caleffi V, Coscia V. Finite volume and weno scheme in one-dimensional vascular system modelling. *Computers and Mathematics with Applications* 2008; **56**:2382–2397, doi:10.1016/J.camwa.2008.05.039.
17. Alastruey J, Parker KH, Peiró J, Sherwin SJ. Lumped parameter outflow models for 1-d blood flow simulations: Effect on pulse waves and parameter estimation. *Commun. Comp. Phys.* 2008; **4**:317–336.
18. Cavallini N, Coscia V. One-dimensional modelling of venous pathologies: Finite volume and weno schemes. *Advances in Mathematical Fluid Mechanics*, Rannacher R, Sequeira A (eds.). Springer Berlin Heidelberg, 2010; 147–170. URL http://dx.doi.org/10.1007/978-3-642-04068-9_9.
19. Willemet M, Lacroix V, Marchandise E. Inlet boundary conditions for blood flow simulations in truncated arterial networks. *Journal of Biomechanics* 2011; **44**(5):897–903, doi:DOI:10.1016/j.jbiomech.2010.11.036. URL http://www.sciencedirect.com/science/article/B6T82-51V8Y64-1/2/eb86e3d4873bd8ec019a622d0c33ca36
20. Marchandise E, Chevaugeon N, Remacle JF. Spatial and spectral superconvergence of discontinuous galerkin method for hyperbolic problems. *Journal of Computational and Applied Mathematics* 2008; **215**(2):484–494, doi:DOI:10.1016/j.cam.2006.03.061. URL http://www.sciencedirect.com/science/article/B6TYH-4MN3V8R-3/2/0bb0cd0d831f13f6105135c1f6c77587 Proceedings of the Third International Conference on Advanced Computational Methods in Engineering (ACOMEN 2005).
21. Fernández MA, Gerbeau JF, Grandmont C. A projection semi-implicit scheme for the coupling of an elastic structure with an incompressible fluid. *International Journal for Numerical Methods in Engineering* 2007; **69**(4):794–821, doi:10.1002/nme.1792.
22. van de Vosse F, de Hart J, van Oijen C, Bessems D. Finite-element-based computational methods for cardiovascular fluid-structure interaction. *Journal of Engineering Mathematics* 2003; **47**:335–368.
23. Saito M, Ikenaga Y, Matsukawa M, Watanabe Y, Asada T, Lagrée PY. One-dimensional model for propagation of a pressure wave in a model of the human arterial network: Comparison of theoretical and experimental. *Journal of Biomechanical Engineering* Dec 2011; **133**, doi:10.1115/1.4005472.
24. Olufsen MS, Peskin CS, Kim WY, Pedersen EM, Nadim A, Larsen J. Numerical simulation and experimental validation of blood flow in arteries with structured-tree outflow conditions. *Annals of Biomedical Engineering* 2000; **28**:1281–1299.
25. Fullana JM, Zaleski S. A branched one-dimensional model of vessel networks. *J. Fluid. Mech.* 2009; **621**:183–204.
26. Pindera MZ, Ding H, Athavale MM, Chen Z. Accuracy of 1d microvascular flow models in the limit of low reynolds numbers. *Microvascular Research* 2009; **77**(3):273–280, doi:DOI:10.1016/j.mvr.2008.11.006. URL http://www.sciencedirect.com/science/article/B6WN8-4V59W3D-1/2/34024497531a550ed28ec3a5aeefc401
27. de Saint Venant AJC. Théorie du mouvement non-permanent des eaux, avec application aux crues des rivières et à l'introduction des marées dans leur lit. *Comptes Rendus de l'Académie des Sciences* 1871; **73**:147–154.
28. Goutal N, Maurel F. A finite volume solver for 1D shallow-water equations applied to an actual river. *International Journal for Numerical Methods in Fluids* 2002; **38**:1–19, doi:10.1002/fld.201.
29. Burguete J, García-Navarro P, Murillo J. Friction term discretization and limitation to preserve stability and conservation in the 1d shallow-water model: Application to unsteady irrigation and river flow. *International Journal for Numerical Methods in Fluids* 2008; **58**(4):403–425, doi:10.1002/fld.1727.
30. Delestre O, Cordier S, James F, Darboux F. Simulation of rain-water overland-flow. *Proceedings of the 12th International Conference on Hyperbolic Problems,* University of Maryland, College Park (USA), 2008, E. Tadmor, J.-G. Liu and A. Tzavaras Eds., Proceedings of Symposia in Applied Mathematics 67, Amer. Math. Soc., 537–546, 2009.
31. Delestre O, James F. Simulation of rainfall events and overland flow. *Proceedings of X International Conference Zaragoza-Pau on Applied Mathematics and Statistics,* Jaca, Spain, september 2008, Monografías Matemáticas García de Galdeano, 2009.
32. Tatard L, Planchon O, Wainwright J, Nord G, Favis-Mortlock D, Silvera N, Ribolzi O, Esteves M, Huang CH. Measurement and modelling of high-resolution flow-velocity data under simulated rainfall on a low-slope sandy soil. *Journal of Hydrology* Jan 2008; **348**(1-2):1–12, doi:10.1016/j.jhydrol.2007.07.016.
33. Valiani A, Caleffi V, Zanni A. Finite volume scheme for 2D shallow-water equations. Application to Malpasset dam-break. *the* 4^{th} *CADAM Workshop, Zaragoza*, 1999; 63–94.

34. Valiani A, Caleffi V, Zanni A. Case Study : Malpasset Dam-Break Simulation using a Two-Dimensional Finite Volume Methods. *Journal of Hydraulic Engineering* May 2002; **128**(5):460–472.
35. Sampson J, Easton A, Singh M. Modelling the effect of proposed channel deepening on the tides in Port Phillip Bay 2005; URL http://hdl.handle.net/1959.3/2405.
36. Dutykh D. Modélisation mathématique des tsunamis. PhD Thesis, École normale supérieure de Cachan 2007.
37. Popinet S. Quadtree-adaptative tsunami modelling. *Ocean Dynamics* May 2011; 1–25,doi:10.1007/s10236-011-0438-z.
38. Bermudez A, Vazquez ME. Upwind methods for hyperbolic conservation laws with source terms. *Computers & Fluids* 1994; **23**(8):1049 – 1071, doi:DOI:10.1016/0045-7930(94)90004-3. URL http://www.sciencedirect.com/science/article/B6V26-47YMXJT-16/2/4485b4adb616198b768daff17225866
39. Bermúdez A, Dervieux A, Desideri JA, Vázquez ME. Upwind schemes for the two-dimensional shallow water equations with variable depth using unstructured meshes. *Computer Methods in Applied Mechanics and Engineering* 1998; **155**(1-2):49 – 72, doi:DOI:10.1016/S0045-7825(97)85625-3. URL http://www.sciencedirect.com/science/article/B6V29-3WN739F-4/2/3120ee07ea5c43b3318fbfb6c05d2dde
40. LeVeque RJ. Balancing source terms and flux gradients in high-resolution godunov methods: The quasi-steady wave-propagation algorithm. *Journal of Computational Physics* 1998; **146**(1):346 – 365, doi:DOI:10.1006/jcph.1998.6058. URL http://www.sciencedirect.com/science/article/B6WHY-45J58TW-22/2/72a8af8c9e23f63b0df9484475f7e2d
41. Jin S. A steady-state capturing method for hyperbolic systems with geometrical source terms. *M2AN* Jul 2001; **35**(4):631–645, doi:10.1051/m2an:2001130. URL http://dx.doi.org/10.1051/m2an:2001130.
42. Greenberg JM, LeRoux AY. A well-balanced scheme for the numerical processing of source terms in hyperbolic equation. *SIAM Journal on Numerical Analysis* 1996; **33**:1–16.
43. Gosse L. A well-balanced flux-vector splitting scheme designed for hyperbolic systems of conservation laws with source terms. *Computers & Mathematics with Applications* 2000; **39**(9-10):135 – 159, doi:DOI:10.1016/S0898-1221(00)00093-6. URL http://www.sciencedirect.com/science/article/B6TYJ-40NFTJN-D/2/320458e48d7fbefdf910aaf251d7255c
44. Gallouët T, Hérard JM, Seguin N. Some approximate godunov schemes to compute shallow-water equations with topography. *Computers & Fluids* 2003; **32**:479–513.
45. Kurganov A, Levy D. Central-upwind schemes for the saint-venant system. *Mathematical Modelling and Numerical Analysis* 2002; **36**:397–425.
46. Perthame B, Simeoni C. A kinetic scheme for the Saint-Venant system with a source term. *Calcolo* 2001; **38**:201–231. URL http://dx.doi.org/10.1007/s10092-001-8181-3, 10.1007/s10092-001-8181-3.
47. Audusse E, Bouchut F, Bristeau MO, Klein R, Perthame B. A fast and stable well-balanced scheme with hydrostatic reconstruction for shallow water flows. *SIAM J. Sci. Comput.* 2004; **25**(6):2050–2065, doi:10.1137/S1064827503431090.
48. Bouchut F. *Nonlinear stability of finite volume methods for hyperbolic conservation laws, and well-balanced schemes for sources*, vol. 2/2004. Birkhäuser Basel, 2004, doi:10.1007/b95203.
49. Vàzquez-Cendòn ME. Improved treatment of source terms in upwind schemes for the shallow water equations in channels with irregular geometry. *Journal of Computational Physics* 1999; **148**:497–526.
50. Chinnayya A, LeRoux AY. A new General Riemann Solver for the Shallow Water equations, with friction and topography. URL http://www.math.ntnu.no/conservation/1999/021.html, 1999. Preprint.
51. Lukáčová-Medvid'ová M, Vlk Z. Well-balanced finite volume evolution Galerkin methods for the shallow water equations with source terms. *International Journal for Numerical Methods in Fluids* 2005; **47**(10-11):1165–1171.
52. Lukáčová-Medvid'ová M, Teschke U. Comparison study of some finite volume and finite element methods for the shallow water equations with bottom topography and friction terms. *J. Appl. Mech. Math. (ZAMM)* 2006; **86**(11):874–891, doi:10.1002/zamm.200510280.
53. Lee SH, Wright NG. Simple and efficient solution of the shallow water equations with source terms. *International Journal for Numerical Methods in Fluids* 2010; **63**:313–340, doi:10.1002/fld.2071.
54. Hou TY, LeFloch PG. Why nonconservative schemes converge to wrong solutions: error analysis. *Mathematics of Computation* Apr 1994; **62**(206):497–530.
55. Berthon C, Coquel F. Nonlinear projection methods for multi-entropies navier-stokes systems. *Mathematics of Computation* 2007; **76**:1163–1194.
56. Castro MJ, LeFloch PG, Luz Muñoz Ruiz M, Parés C. Why many theories of shock waves are necessary: Convergence error in formally path-consistent schemes. *Journal of Computational Physics* 2008; **227**(17):8107–8129, doi:DOI:10.1016/j.jcp.2008.05.012. URL http://www.sciencedirect.com/science/article/B6WHY-4SMNY18-1/2/a96e0bdf121ac34604742fdc9165bd07

DOI: 10.1002/fld

57. Lagrée PY, Lorthois S. The rns/prandtl equations and their link with other asymptotic descriptions. application to the computation of the maximum value of the wall shear stress in a pipe. *Int. J. Eng. Sci.* 2005; **43**(3–4):352–378.
58. Zagzoule M, Khalid-Naciri J, Mauss J. Unsteady wall shear stress in a distensible tube. *J. Biomechanics* 1991; **24**(6):435–439.
59. Kundu PK, Cohen IM. *Fluid Mechanics, Third Edition*. 2004.
60. Kundu PK, Cohen IM. *Fluid Mechanics, Fourth Edition*. 2008.
61. Castro MJ, Pardo Milanés A, Parés C. Well-balanced numerical schemes based on a generalized hydrostatic reconstruction technique. *Mathematical Models and Methods in Applied Sciences* 2007; **17**(12):2065–2113.
62. Noelle S, Xing Y, Shu CW. High-order well-balanced finite volume weno schemes for shallow water equation with moving water. *Journal of Computational Physics* 2007; **226**(1):29 – 58, doi:DOI:10.1016/j.jcp.2007.03.031. URL http://www.sciencedirect.com/science/article/B6WHY-4NG3TH4-3/2/546ff3d247ae9db8ed41e3de935ee892
63. Thanh MD, Fazlul Karim M, Ismail AIM. Well-balanced scheme for shallow water equations with arbitrary topography. *Int. J. Dynamical Systems and Differential Equations* 2008; **1**(3):196–204.
64. Bouchut F, Morales T. A subsonic-well-balanced reconstruction scheme for shallow water flows. URL http://www.math.ntnu.no/conservation/2009/032.html, 2009. Preprint.
65. Fiedler RF, Ramirez JA. A numerical method for simulating discontinuous shallow flow over an infiltrating surface. *International Journal for Numerical Methods in Fluids* 2000; **32**:219–240.
66. Bristeau MO, Coussin B. Boundary conditions for the shallow water equations solved by kinetic schemes. *Technical Report 4282*, INRIA Oct 2001.
67. Liang Q, Marche F. Numerical resolution of well-balanced shallow water equations with complex source terms. *Advances in Water Resources* 2009; **32**(6):873 – 884, doi:DOI:10.1016/j.advwatres.2009.02.010. URL http://www.sciencedirect.com/science/article/B6VCF-4VR9FHT-3/2/5218868dcfded7d34380666f23000855
68. Mangeney-Castelnau A, Bouchut F, Vilotte JP, Lajeunesse E, Aubertin A, Pirulli M. On the use of saint-venant equations to simulate the spreading of a granular mass. *Journal of Geophysical Research* 2005; **110**:B09 103.
69. Mangeney A, Bouchut F, Thomas N, Vilotte JP, Bristeau MO. Numerical modeling of self-channeling granular flow and of their levee-channel deposits. *Journal of Geophysical Research* May 2007; **112**(F2):F02 017, doi: 10.1029/2006JF000469.
70. Harten A, Lax PD, van Leer B. On upstream differencing and godunov-type schemes for hyperbolic conservation laws. *SIAM Review* Jan 1983; **25**(1):35–61.
71. Marche F, Bonneton P, Fabrie P, Seguin N. Evaluation of well-balanced bore-capturing schemes for 2D wetting and drying processes. *International Journal for Numerical Methods in Fluids* 2007; **53**:867–894, doi:10.1002/fld.1311.
72. Marche F, Berthon C. A positive preserving high order vfroe scheme for shallow water equations: A class of relaxation schemes. *SIAM Journal on Scientific Computing* Aug 2008; **30**(5):pp. 2587–2612. URL http://hal.archives-ouvertes.fr/hal-00370486/en/, 75M12, 35L65, 65M12.
73. Audusse E. Schémas cinétiques pour le système de Saint-Venant. Master's Thesis, Université Paris 6 1999.
74. Audusse E, Bristeau MO. A well-balanced positivity preserving "second-order" scheme for shallow water flows on unstructured meshes. *Journal of Computational Physics* 2005; **206**:311–333, doi:10.1016/j.jcp.2004.12.016.
75. Delestre O. Simulation du ruissellement d'eau de pluie sur des surfaces agricoles/ rain water overland flow on agricultural fields simulation. PhD Thesis, Université d'Orléans (in French), available from TEL: tel.archives-ouvertes.fr/INSMI/tel-00531377/fr Jul 2010.
76. LeVeque RJ. *Finite volume methods for hyperbolic problems*. Cambridge Texts in Applied Mathematics, Cambridge University Press: Cambridge, 2002.
77. van Leer B. Towards the ultimate conservative difference scheme. V. A second-order sequel to Godunov's method. *Journal of Computational Physics* 1979; **32**(1):101 – 136, doi:DOI:10.1016/0021-9991(79)90145-1. URL http://www.sciencedirect.com/science/article/B6WHY-4DD1N8T-C5/2/9b051d1cfcff715a3d0f4b7b7b0397c
78. Delestre O, Marche F. A numerical scheme for a viscous shallow water model with friction. *J. Sci. Comput.* 2010; doi:DOI:10.1007/s10915-010-9393-y.
79. Harten A, Osher S, Engquist B, Chakravarthy SR. Some results on uniformly high-order accurate essentially nonoscillatory schemes. *Applied Numerical Mathematics* 1986; **2**(3-5):347 – 377, doi:DOI:10.1016/0168-9274(86)90039-5. URL http://www.sciencedirect.com/science/article/B6TYD-45GVV8T-J/2/830ca2dce5e3fb34ace9fa53ae5ab76b special Issue in Honor of Milt Rose's Sixtieth Birthday.
80. Harten A, Engquist B, Osher S, Chakravarthy SR. Uniformly High Order Accurate Essentially Non-oscillatory Schemes, III. *Journal of Computational Physics* Aug 1987; **71**:231–303.
81. Shu CW, Osher S. Efficient implementation of essentially non-oscillatory shock-capturing schemes. *Journal of Computational Physics* 1988; **77**(2):439 – 471, doi:DOI:10.1016/0021-9991(88)90177-5. URL http://www.sciencedirect.com/science/article/B6WHY-4DD1T6W-MM/2/bef99e4b67bd7132c8af1984c34ce57

82. Bouchut F, Ounaissa H, Perthame B. Upwinding of the source term at interfaces for euler equations with high friction. *Computers and Mathematics with Applications* 2007; **53**:361–375, doi:10.1016/j.camwa.2006.02.055.
83. Noelle S, Pankratz N, Puppo G, Natvig JR. Well-balanced finite volume schemes of arbitrary order of accuracy for shallow water flows. *Journal of Computational Physics* 2006; **213**(2):474 – 499, doi:DOI:10.1016/j.jcp.2005.08.019. URL http://www.sciencedirect.com/science/article/B6WHY-4HB4DN4-1/2/15c5962d035c22b4fee10302b2606fa6
84. Stoker JJ. *Water Waves: The Mathematical Theory with Applications*. Interscience Publishers, New York, USA, 1957.
85. LeVeque RJ. *Numerical methods for conservation laws*. Lectures in mathematics ETH Zurich, 1992.
86. Ockendon H, Tayler AB. *Inviscid Fluid Flows*. 1983.
87. Kirkman R, Moore T, Adlard C. *The Walking Dead*. Image Comics, 2003.
88. Womersley J. On the oscillatory motion of a viscous liquid in thin-walled elastic tube: I. *Philos. Mag.* 1955; **46**:199–221.